FERRITE-POLYMER NANOCOMPOSITES: STRUCTURAL, ELECTRICAL, MAGNETIC AND EMI SHIELDING PROPERTIES

Abstract

Utilizing polyaniline (PANI) filler inside of a ferrite (NiCuZnFe2O4) matrix, electromagnetic absorbent materials that blend organic and inorganic components have been successfully created. These NiCuZn ferrite-PANI nanocomposites were created by mechanically milling ferrite. X-ray diffraction (XRD), Fourier infrared spectroscopy (FTIR), and scanning electron microscopy were used to examine the structural and morphological features of these nanocomposites (SEM). The X-band (8.2-12.4 GHz) and Ku band (12-18 GHz) frequency ranges' electromagnetic characteristics and absorption patterns were investigated. The results show that for nanocomposites, the values of the real (ε′) and imaginary permittivity (ε″) and imaginary permeability (μ″) increase, while the value of real permeability (μ′) decreases as the filler content increases. The morphology, conductivity, and microwave absorption characteristics of the final materials are strongly influenced by parameters such as the amount and particle size of PANI and NCZ. It was shown that the addition of PANI increases overall shielding efficacy as well as reflection loss (RL) (SEtot). The nanocomposite that has the maximum RL, -41.72 dB, has 50% PANI by weight. The higher magnetic and dielectric losses brought on by the incorporation of conductive PANI filler inside the ferrite matrix are what are responsible for these nanocomposites' enhanced electromagnetic absorption capacities. For the creation of high-performance microwave-absorbing and electromagnetic shielding materials, the ability to manipulate the electromagnetic characteristics of these composite materials offers considerable potential.

Keywords: Nanocomposites; Electromagnetic absorption; Reflection loss; Permittivity; permeability;

Authors

P. Raju
Geethanjali College of Engineering and Technology
Cheeryal, Hyderabad, India.

CH. Kalyani
Geethanjali College of Engineering and Technology
Cheeryal, Hyderabad, India.

G. Neeraja Rani
Geethanjali College of Engineering and Technology
Cheeryal, Hyderabad, India.

M. Kanaka Durga
Geethanjali College of Engineering and Technology
Cheeryal, Hyderabad, India.

J. Anjaiah
Geethanjali College of Engineering and Technology
Cheeryal, Hyderabad, India.

S. Katlakunta
Department of Physics
University College of Science
Osmania University
Hyderabad, India.

I. INTRODUCTION

In comparison to conventional polymer composites, magnetic polymer nanocomposites provide a number of benefits and are thus extremely relevant. Nanocomposites can accomplish the necessary qualities with a substantially less amount of filler material than micron-sized composites, which frequently need a high filler percentage. Lower density and better processability are the outcomes of this. Compared to micron-sized particles, nanoparticles have different benefits because they may display special magnetic, optical, thermal, electrical, and mechanical capabilities. Furthermore, compared to materials that are micron in size, magnetic characteristics including coercivity, saturation magnetization, and frequency-dependent permeability in nanoparticles are very different.

Magnetic polymer composites are utilised in a variety of industries, such as the automotive and healthcare sectors, where they act as sensors and are employed to reduce electromagnetic interference (EMI). Particularly electronic equipment produce radiofrequency waves that can interfere with the operation of both their internal parts and other electronic devices nearby. Electronic components must be packed more closely as electronic gadgets get smaller in today's world, which makes electromagnetic interference a bigger problem. An electromagnetic wave experiences reflection and absorption when it comes into contact with a conducting surface.

The capacity of a material to shield electromagnetic energy, whether it is preventing unwanted energy from entering a system or preventing it from escaping, is known as its shielding effectiveness. Shielding effectiveness encompasses losses due to absorption, reflection, and multiple reflections [1]. Achieving EMI suppression over a wide range of frequencies requires the ability to adjust impedance (Z), which relies on the tunability of complex permeability and complex permittivity. The conductivity of a material plays a pivotal role in its effectiveness in shielding electromagnetic energy.

Ferrites, metals, and capacitors are frequently used to reduce electromagnetic interference (EMI), although they have substantial disadvantages due to their stiffness, weight, and susceptibility to corrosion [2]. Using materials like ferrite and conducting polymers, among others, some researchers have looked into the absorbing qualities of single-component EMI wave absorbers [3, 4]. Single-component materials, however, offer less promise than composite materials because of their lower absorption efficiency and smaller bandwidth. The creation of novel composite materials can overcome these constraints. Ferrite/polymer nanocomposites are a better option among composite materials because magnetic nanoparticles mixed with conducting and insulating polymers provide lightweight and flexible alternatives to bulky metal components. The capacity of magnetic-polymer nanocomposites to manage fundamental variables like loss tangents and impedance matching, which are essential in microwave devices, is another important benefit. The magnetic and eddy current losses, which depend on the material's resistivity, are the main factors that affect the loss tangent, which assesses the inefficiency of a magnetic system. The resistance of magnetic nanoparticles is increased by the addition of conducting polymer, lowering eddy current losses. In nanocomposite materials, these characteristics may be successfully controlled by nanoparticle size distribution and dispersion within the matrix. Typically, magnetic losses in composite materials are impacted by variables including material grain structure and domain wall resonances.

The main reason for signal attenuation during circuit transmission is an impedance mismatch between the source and the load. It is possible to attain desired impedance values at particular frequencies by modifying the characteristics of nanocomposites, hence reducing signal attenuation. By changing the kind and amount of polymer scattered among the magnetic nanoparticles, the impedance of nanocomposite materials may be precisely controlled. Ferrimagnetic nanoparticles and conducting polymers are combined to produce an important nanocomposite with a distinctive fusion of electrical and magnetic characteristics. Nanocomposite materials are suited for usage as electromagnetic shielding materials due to this property. This is owing to the fact that electromagnetic waves are made up of perpendicular electric (E) and magnetic (H) fields. Impedance, which is the ratio of the E to the H factors, is very important in shielding applications. Conducting polymer materials can efficiently block electromagnetic waves produced by electric sources in the case of ferrite/polymer nanocomposites, but magnetic materials are better at blocking electromagnetic waves produced by magnetic sources.

Electromagnetic Interference (EMI) shielding mainly uses reflection as its main technique. The shielding material must have mobile charge carriers, such as electrons or holes, that may interact with the electromagnetic fields present in the radiation in order to successfully reflect this kind of radiation. As a result, EMI shields are frequently constructed from electrically conductive materials, with a degree of conductivity that typically equates to a volume resistivity of around 1 cm [5]. Absorption is a secondary EMI shielding technique. The shielding material must have electric and/or magnetic dipoles that interact with the electromagnetic fields of the radiation for the radiation to be effectively absorbed. Therefore, a system that combines both magnetic and conductive components can be used as an EMI shielding material [6].

The development of polymer-inorganic filler composites has received significant research attention in order to protect precision equipment against electromagnetic microwave interference, lower radiation exposure to people, and shield against electromagnetic interference. Low density, high hardness, structural plasticity, and enhanced electromagnetic characteristics are only a few benefits offered by nanocomposites made of conductive polymers and magnetic particles [7-9]. Due to the synergistic combination of conductive polyaniline and magnetic ferrite, composites of these two materials particularly show potential for these applications.

In this investigation, it will be determined whether there is a quantitative correlation between the magnetic and dielectric characteristics of ferrite/polymer composites and their capacity to absorb microwaves in the X-band (8.2 - 12.4 GHz) and Ku-band (12.4-18.0 GHz) frequency ranges.

For more than 70 years, the study of magnetic materials has relied heavily on ferrites, magnetic ceramics predominantly made of iron oxide. They are widely utilised in a variety of applications and considerably aid in the development of electronics. Despite their long history, ferrites are still undergoing research, finding new uses, and seeing advancements in preparation techniques.

Due to their superior electromagnetic characteristics, NiCuZn ferrites have become more popular in microwave applications [10]. Compared to MnZn ferrites, they have

improved high-frequency properties, while NiZn ferrites have lower densification temperatures. Producing multilayer ferrite chip inductor components for use in LC filters, EMI filters, AC chokes for active devices, matching circuits, and other circuits has recently attracted attention to NiCuZn ferrite. Ferrites are also essential components of electronic devices such as audiovisual equipment, personal wireless communication systems, vehicle telephony, and many more.

Numerous zinc ferrite [11], barium ferrite [12–14], cobalt ferrite [15, 16], iron oxide [17], and manganese-zinc ferrite [18–20] nanocomposites of polyaniline have also been discovered. Core-shell architectures are common in these nanocomposites, where polyaniline shells encase the ferrite nanoparticles. Despite having shown microwave absorption and electromagnetic shielding abilities, ferrite nanoparticles' propensity to agglomerate, brought on by their tiny size and magnetic characteristics, might restrict their efficacy. This aggregation significantly reduces the strength and frequency range of electromagnetic-absorbing nanocomposites, which offers a considerable problem in their practical use.

EMI shielding in the X-band (8.2-12.4 GHz) frequency range has been covered extensively in research articles employing a variety of materials, including carbon-based materials, carbon-reinforced polymer composites, polymer composites, metal composites, and magnetic materials. These materials have found use in defence monitoring, aviation control, weather forecasting, high-resolution imaging radars, and military communication satellites [21–23]. Although research explicitly focused on absorbers for this frequency range are few [24, 25], the Ku-band frequency range is commonly employed in satellite communication. Notably, to the best of our knowledge, there haven't been any published investigations on ferrite/polymer nanocomposites microwave absorbers in the literature.

In this work, we developed different nanocomposites by mechanically milling Polyaniline (PANI) into a $Ni_{0.48}Cu_{0.12}Zn_{0.4}Fe_2O_4$ (NCZ) matrix. NCZ is well suited for use in microwave devices and microwave absorption fields because of its high saturation magnetization, exceptional chemical stability, and resistance to corrosion. We looked at how the volume percentage of the polymer affected the complex permittivity (ε' & ε'') and permeability (μ' & μ'') frequency dispersion properties in the nanocomposite powders. Analysis and discussion of the experiments' findings were conducted. We also looked at the nanocomposite samples' microwave absorption characteristics at various frequencies and sample thicknesses. Computer simulations were used to perform this experiment utilising a model of a single-layered plane wave absorber supported by a perfect conductor. We also determined the ideal thicknesses and matching frequencies that minimise reflection for the best-performing sample, which included 50% PANI.

II. EXPERIMENTAL PROCEDURES

1. **Synthesis of NCZ Ferrite:** The nickel nitrate [Ni $(NO_3)_2$•$6H_2O$], zinc nitrate [Zn $(NO_3)_2$•$6H_2O$], copper nitrate [Cu $(NO_3)_2.6H_2O$], and ferric nitrate [Fe $(NO_3)_3$•$9H_2O$] were exceedingly pure chemicals [99.9 percent purity] that were used to make the nickel, zinc, copper, and zinc, or NCZ, nanopowder. In 50 cc of de-ionized water, these compounds were dissolved. Since pH control is essential for the manufacture of nanopowder, sodium hydroxide (NaOH) was added to the solution to keep its pH at or near ~12. The resultant precipitate was then put into double-walled digesting tanks with

an exterior layer made of high-strength Ultem polyetherimide and an inner liner and lid made of Teflon PFA. Next, a microwave-hydrothermal (M-H) treatment lasting 45 minutes at 160°C was performed. A microwave-accelerated reaction system (MARS-5, CEM Corp., Mathews, NC) was used for the M-H treatment. It operates at a microwave frequency of 2.45 GHz and has a power range of 0% to 100% (1200±50 W). For temperature control and monitoring during the synthesis process, an optical probe was attached to the reaction vessel. The product was then centrifuged to separate it, rinsed many times with deionized water, and dried in an oven at 60°C for an extended period of time. A yield of 96 percent was obtained after the powders were weighed and the percentage yield was calculated by comparing the quantity of crystallisation to the anticipated yield based on the volume and concentration of the starting solution. Subsequently, the as-synthesized powders were characterized using X-ray diffraction (XRD) with a Philips PW-1730 X-ray diffractometer.

2. **Synthesis of PANI:** PANI was created through a multi-step process. Initially, 100 ml of an equal mixture of aniline and hydrochloric acid in distilled water was used to create aniline hydrochloride. Ammonium peroxydisulfate (APS), at a concentration of 0.25M, was simultaneously dissolved in 100 ml of water. One hour of room temperature (25°C) standing was given to both solutions. They were then mixed together in a beaker, agitated with a mechanical stirrer, and left unattended to promote polymerization. On the second day, the PANI precipitate was similarly filtered, collected, washed with 0.2 M HCl in 300 ml parts, and rinsed with acetone. The powdered polyaniline (emeraldine) hydrochloride was produced and dried twice, once in the open air and once in a vacuum at 60°C.

3. **Synthesis of NCZ-PANI Nanocomposites:** In order to generate nanocomposites with the formula (1-x)NCZ + xPANI, where x varied from 0 to 1, the as-synthesised nanopowders of NCZ and PANI were mixed. According to their various compositions, the resultant samples were given the names NCZ, NP1, NP2, NP3, NP4, NP5, and PANI. A high-energy planetary ball mill made by Retsch Co. was then used to mechanically grind the combined particles. Ten 12 mm tungsten carbide balls and a hardened tungsten carbide (WC) vial were used in this 30-hour-long milling procedure. The mill ran at a speed of 400 rpm with a 40-minute break in between processes, with a ball-to-powder mass charge ratio of 14:1. The milled powders were then annealed for 30 minutes in an environment of air at 110°C. X-ray diffraction (XRD), scanning electron microscopy (SEM), and Fourier-transform infrared spectroscopy (FTIR) utilising Brucker tensor 27 were used to characterise the materials.

The fluctuations of microwave absorption in decibels (dB) vs frequency in the range of 8-18 GHz were evaluated for the composite samples in order to explore the microwave absorption features. This was done with the help of an Agilent 8722ES vector network analyzer. The NCZ-PANI nanocomposite samples were designed to exactly fit inside the X-band (WR90) and Ku-band (WR62) waveguides used for microwave experiments. In the composite samples, complex scattering parameters S11 or S22 and S21 or S12 relating to reflection and transmission, were measured. To remove inaccuracies in both the forward and reverse directions relating to directivity, source match, load match, isolation, etc., first two-port calibrations were done on the test setup. Then, using Agilent software module 85071 and the method described in the HP product note, complex permittivity (ε' & ε") and permeability (μ' & μ") were calculated from the

observed scattering parameters. Following that, the samples' reflection loss was estimated and examined.

III. RESULTS AND DISCUSSIONS

The NCZ-PANI nanocomposites' as-prepared X-ray diffraction (XRD) patterns are shown in Figure 1. CuK radiation with a wavelength () of 1.5418, encompassing the 2 range from 10° to 80° with a 0.03° step size, was used to acquire these patterns at ambient temperature. At 40 kV and 30 mA, the XRD instrument was in use. The ferrite phase may be clearly seen as discrete crystalline peaks in the XRD patterns of the nanocomposites. Notably, the presence of the polymer has an impact on the intensity of these ferrite peaks. In particular, the presence of polymer causes the intensity of the ferrite peaks to decrease, and the reverse is also true. Additionally, the diffused peak connected to PANI loses intensity as the ferrite percentage of the composites rises. The interaction of ferrite nanoparticles with the PANI chains is what causes this effect. By looking at the graphs, it is clear that adding more polymer causes the diffraction peaks to widen. The Debye-Scherrer formula ($L = K\lambda/\beta \cos\theta$, K is a constant, λ wavelength of X-rays, β the full-width half maximum and θ the diffraction angle) was used to calculate the mean NCZ crystallite size for each sample. This formula, uses the diffraction line's full width at half maximum (FWHM) at half the maximum intensity as determined at the peak with the highest intensity (3 1 1). This formula was used to do calculations, and the outcomes are shown in Table 1. It is noteworthy that the composites' crystallite size is in the nano range and that it gets smaller as the PANI concentration rises. The diffraction peak (3 1 1) is also shifted towards the lower Bragg angle side by an increase in PANI concentration. This shift is a result of tension brought on by the presence of ferrite particles and shows that NCZ particles are linked to polymer chains.

The lattice constant (a) for the present samples is calculated by using XRD patterns. For a given set of planes (h k l) and from Bragg's equation 'd' spacing is given by

$$d_{hkl} = \frac{n\lambda}{2\sin\theta} \qquad \text{....(1)}$$

Where n is the order of reflection, λ is the wavelength of radiation and θ is the glancing angle of the incident X-ray beam. For cubic crystals, d_{hkl} is given by

$$d_{hkl} = \frac{a}{\sqrt{h^2+k^2+l^2}} \qquad \text{....(2)}$$

All of the peaks seen in the XRD pattern were taken into account for determining the lattice parameters of the composites, and these values are shown in Table 1. The table clearly shows that the lattice constant drops as the nanocomposite's polymer concentration rises. It's significant to note that while lattice distortion results from the addition of polymer in NCZ, the crystal structure of the ferrite is unaffected.

The bulk density of all the composite samples has been measured accurately (up to 1%) using the Archimedes principle. The bulk density is obtained by using Eq 3

$$b_{bulk} = \frac{M_{air}}{M_{air} - M_{Xylene}} \qquad \text{-- (3)}$$

Where Mair is the mass of the sample in air and MXylene is the mass of the sample in Xylene

Table 1 contains measurements of the nanocomposites' bulk densities. The bulk density of the nanocomposites is seen to decrease as the polymer concentration rises. This is because the molecular weight of ferrite surpasses that of PANI, leading to this tendency.

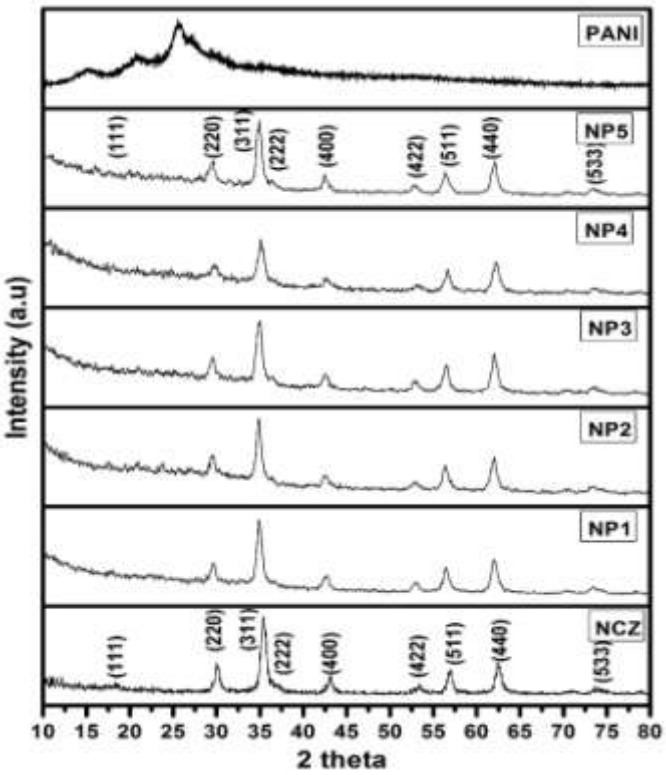

Figure 1: XRD patterns of NCZ-PANI nanocomposites. Reproduced with permission from, Raju, P., P. Neelima, G. Neeraja Rani, and M. Kanakadurga. "Enhanced microwave absorption properties of Ni0. 48Cu0. 12Zn0. 4Fe2O4+ polyaniline nanocomposites." Journal of Physics and Chemistry of Solids 154 (2021): 110048.

In order to examine the chemical composition of the nanocomposites, FTIR spectroscopy was employed. The FTIR spectra of ferrite (NCZ) and nanocomposites with various ratios of polyaniline to ferrite are shown in Figure 2.

The absorption bands in the 100 to 1000 cm-1 region of the infrared spectra of solid materials are often connected to the oscillations of ions inside the crystal lattice. Depending on the configuration of oxygen atoms nearby, metal ions in ferrites are often found in two separate sublattices known as tetrahedral and octahedral sites. A high-frequency band (600-550 cm-1) attributable to the inherent vibrations of tetrahedral sites and a low-frequency band (440-400 cm-1) assigned to octahedral sites define the vibrational spectra of spinel ferrites (MFe2O4) [26. 17]. The vibrations of the C-O, C-O-C, and C-H groups present in the surfactant are responsible for the bands at 1635 cm-1, 1400 cm-1, and 1122 cm-1 seen in the ferrite spectrum. [28, 29]

Peaks for polyaniline may be seen at 1612, 1558, 1473, 1145, 837, 617, and 503 cm-1. The quinoid ring's C-N vibration is represented by the band at 1612 cm-1, while the benzenoid ring's C-C stretching vibration is represented by the bands at 1558 cm-1 and 1473 cm-1, respectively. The stretching of C-N bonds in second aromatic amines is shown by the band at 1145 cm-1. At 837 cm-1, the C-N+ polaron structure is shown to be extending. The polyaniline backbone chain's protonated amine group is responsible for the absorption at 917 cm-1, and the band at 503 cm-1 is related to the aromatic ring's deformation and out-of-plane vibrations of the C-H bond [30].

Figure 2 shows that the typical peaks of both ferrite and polyaniline (PANI) are present in the polyaniline-ferrite nanocomposite samples. Notably, when the PANI concentration rises, the NCZ ferrite characteristic peak at 561 cm-1 moves. Furthermore, when the weight % of ferrite in the nanocomposite declines, so does the intensity of the 561 cm-1 signal. The composites' bands between 1400 and 1600 and 1130 cm-1 show a connection between ferrite and polyaniline. When compared to the FTIR spectra of pure PANI, all bands in these nanocomposites exhibit small changes, and they all correspond to vibration modes inside the ferrite matrix. This implies that PANI crystallises alongside ferrite nanocrystals. Certain FTIR bands of PANI inside the nanocomposites change as a result of the polymer inclusion in the NCZ matrix. These findings imply that NCZ-PANI nanocomposites may be successfully formed by the interaction of PANI chains with NCZ ferrite.

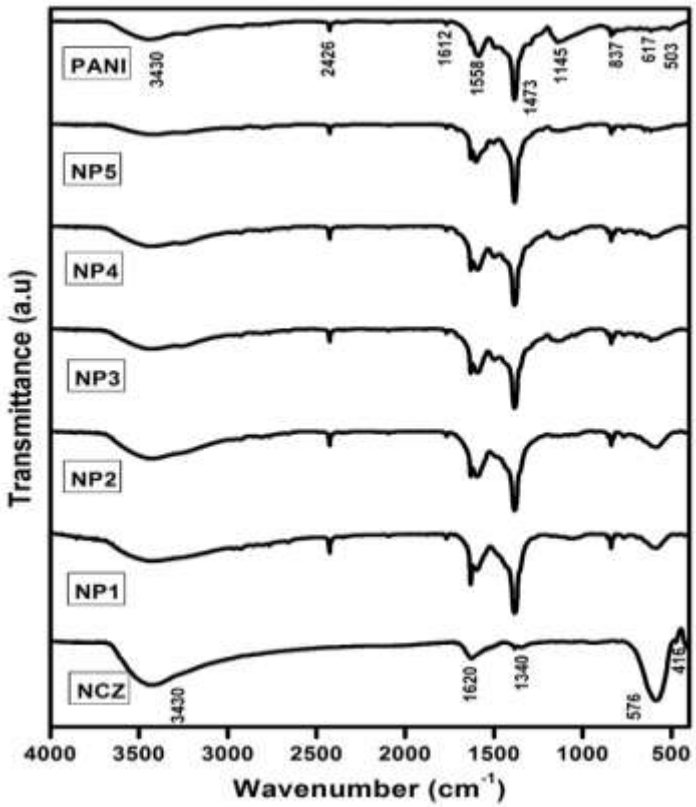

Figure 2: FTIR spectra for NCZ-PANI nanocomposites. Reproduced with permission from, Raju, P., P. Neelima, G. Neeraja Rani, and M. Kanakadurga. "Enhanced microwave absorption properties of Ni0. 48Cu0. 12Zn0. 4Fe2O4+ polyaniline nanocomposites." Journal of Physics and Chemistry of Solids 154 (2021): 110048.

Figure 3 shows the outcomes of the SEM examination that was done to look at the morphologies of NCZ, polyaniline, and their nanocomposite. The ferrite nanoparticles (NCZ) in the SEM picture have an average diameter of around 30 nm and are clearly spherical in form with extensive interparticle aggregation. Polyaniline (NP4) has an average diameter of 60 nm and a length of 100 nm, according to the SEM examination. For effective electron transport, polyaniline creates a tubular shape and tends to form an entangled network. Figures 3.6 (NP3) and 3.7 (NP4) show how ferrite nanoparticles have been assembled on the surface of polyaniline. One potential way the ferrite nanoparticles can adhere to the polyaniline surface is seen in Fig. 3.6 (NP3). The SEM picture of the nanocomposite in Fig. 3.7 (NP4) reveals that the surface of polyaniline is evenly covered in ferrite nanoparticles, with no evidence of ferrite aggregation. The nanocomposites' SEM micrographs show a two-phase system made up of polymer grains (white) and ferrite grains (black). The presence of these two phases was verified using energy-dispersive X-ray spectroscopy. The connection of the NiCuZn ferrite grains is disrupted by the dispersion of polymer grains, changing the magnetic characteristics of the composites.

Using SEM pictures using the equation G=1.5L/MN, where L is the total test line length in cm, M is the magnification, and N is the total number of intercepts, the average grain sizes of the samples were calculated. Table 1 presents the outcomes. It is interesting that, although seeming bigger than the comparable "crystallite" sizes found from X-ray diffraction research, the estimated average grain sizes are in the nanoscale range. This is predicted given that the disordered grain borders, which take up a significant amount of space in nanoparticles, cannot be seen by X-rays, which can only see the crystallites, which are the well-ordered parts of the particles. In addition, many particles may group together, appearing in SEM pictures as a single, bigger particle. By using X-rays, such agglomerations could not be seen. The literature has documented similar observations and explanations [31, 32].

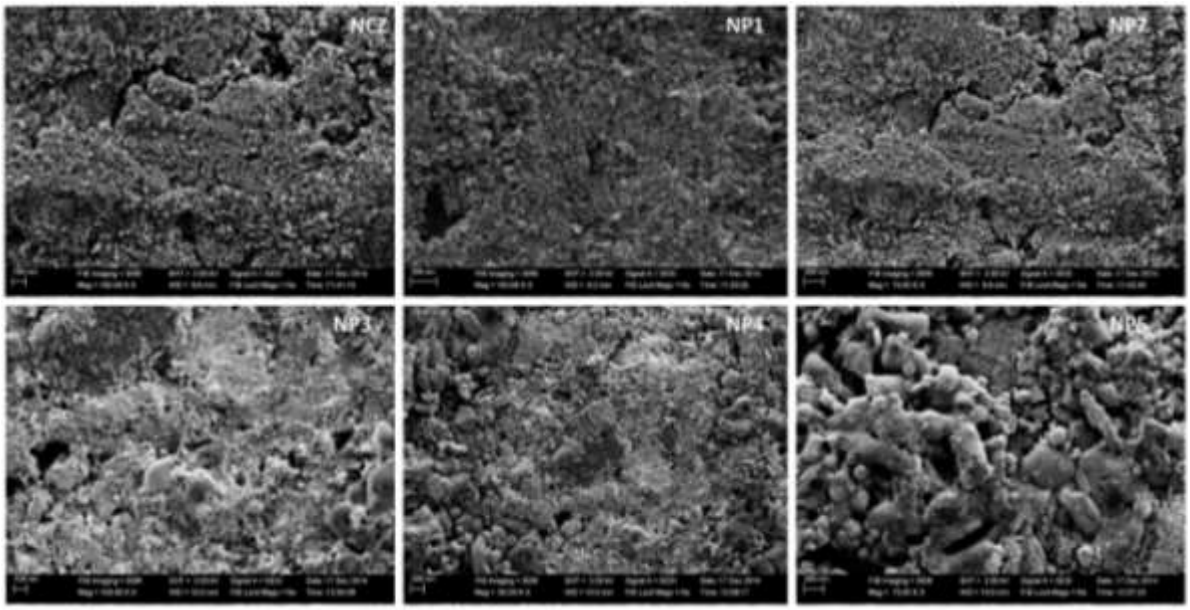

Figure 3: SEM images of NCZ-PANI nanocomposites. Reproduced with permission from, Raju, P., P. Neelima, G. Neeraja Rani, and M. Kanakadurga. "Enhanced microwave absorption properties of Ni0. 48Cu0. 12Zn0. 4Fe2O4+ polyaniline nanocomposites." Journal of Physics and Chemistry of Solids 154 (2021): 110048.

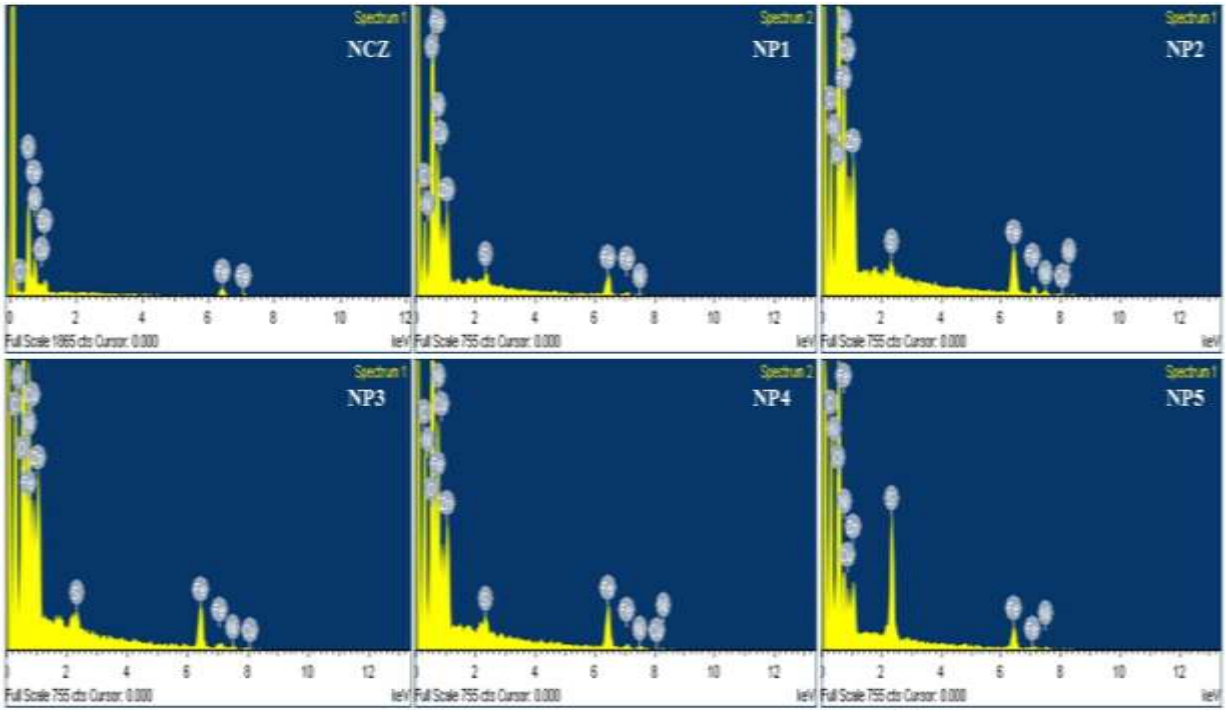

Figure 4: EDS spectra of NCZ-PANI nanocomposites. Reproduced with permission from, Raju, P., P. Neelima, G. Neeraja Rani, and M. Kanakadurga. "Enhanced microwave absorption properties of Ni0. 48Cu0. 12Zn0. 4Fe2O4+ polyaniline nanocomposites." Journal of Physics and Chemistry of Solids 154 (2021): 110048.

Table 1: Structural data of NCZ-PANI nanocomposites

Sample	XRD Crystallite size (nm)	Lattice parameter (Å)	Density g/cm^3	Grain size (nm)
NCZ	35	8.439±0.001	5.25	40
NP1	33	8.424±0.001	5.23	38
NP2	30	8.412±0.001	5.21	35
NP3	29	8.403±0.001	5.13	33
NP4	27	8.402±0.001	5.11	29
NP5	25	8.401±0.001	5.01	27

Table 2 EDS elemental analysis of NCZ-PANI nanocomposites. Reproduced with permission from, Raju, P., P. Neelima, G. Neeraja Rani, and M. Kanakadurga. "Enhanced microwave absorption properties of Ni0. 48Cu0. 12Zn0. 4Fe2O4+ polyaniline nanocomposites." Journal of Physics and Chemistry of Solids 154 (2021): 110048.

NCZ		
Element	Weight%	Atomic%
C K	12.99	28.31
O K	26.95	44.11
Fe L	46.76	21.92
Ni L	6.97	3.11
Cu L	0.47	0.19
Zn L	5.86	2.35
Total	100	100

NP1		
Element	Weight%	Atomic%
C K	17.69	36.12
N K	1.76	3.09
O K	23.68	36.31
S K	0.65	0.50
Fe L	39.80	17.48
Ni L	7.97	3.33
Cu L	0.98	0.38
Zn L	7.47	2.80
Totals	100.00	100

NP2		
Element	Weight%	Atomic%
C K	18.31	36.95
N K	2.51	4.35
O K	23.11	35.01
S K	0.39	0.29
Fe L	36.84	15.99
Ni L	9.72	4.01
Cu L	1.37	0.52
Zn L	7.75	2.87
Totals	100.00	100

NP3		
Element	Weight%	Atomic%
C K	19.85	29.55
N K	14.28	18.23
O K	35.95	40.17
S K	11.15	6.22
Fe L	13.45	4.30
Ni L	2.53	0.77
Cu L	0.49	0.14
Zn L	2.30	0.63
Totals	100.00	100

NP4		
Element	Weight%	Atomic%
C K	26.19	40.93
N K	7.89	10.57
O K	29.74	34.89
S K	6.98	4.08
Fe L	19.97	6.71
Ni L	5.19	1.66
Cu L	0.09	0.03
Zn L	3.96	1.14
Totals	100.00	100

NP5		
Element	Weight%	Atomic%
C K	31.89	49.86
N K	6.46	8.66
O K	24.04	28.22
S K	3.88	2.27
Fe L	22.07	7.42
Ni L	6.61	2.11
Cu L	1.02	0.30
Zn L	4.04	1.16
Totals	100.00	100

The Energy-Dispersive X-ray Spectroscopy (EDS) spectra from the SEM images are shown in Figure 4. These spectra were investigated to identify the distribution of nano ferrite inside the PANI polymer. The NCZ particles were uniformly distributed throughout the polymer, according to these EDS spectra. Notably, when the weight % of NCZ in the NCZ-PANI nanocomposites increases, the intensity of NCZ in the EDS spectra likewise increases, showing that the NCZ particles were evenly distributed throughout the polymer. The NCZ-PANI nanocomposites' constituent weights and atomic percentages are detailed in Table 2.

To evaluate the thermal stability of the nanocomposites and look into interactions between ferrite and polyaniline, thermogravimetric analysis was used. The thermogravimetric curves (TG) of the nanocomposites NCZ and NCZ-PANI are shown in Figure 5. Under an environment of inert nitrogen gas, the materials were heated from 30 to 850°C at a steady rate of 10°C/min. Various PANI-to-ferrite ratios in nanocomposites showed different phases of heat deterioration. Up to 850°C, NiCuZn ferrite showed outstanding thermal stability with just an 8 percent weight loss. The first weight loss at 110°C in the nanocomposites was seen on the TGA curve and was attributable to the elimination of water and other volatile species. This view is in line with Gomes and Oliveira's results [33]. The desorption of water and dopant molecules adsorbed on polyaniline, as well as the breakdown of oligomers, are responsible for weight loss below 250°C [34]. The breakdown of the polyaniline molecular chains is related to the third degradation stage [35]. Small aromatic fragments, substituted aromatic fragments, and extended aromatic fragments are formed after the breakdown of polyaniline backbone chains [33]. As expected, increasing ferrite concentration in the nanocomposites led to enhanced resistance to heat deterioration. These thermograms show improved thermal stability of polyaniline in the nanocomposites, which may be brought on by strong contacts between the surface of the polyaniline and the ferrite.

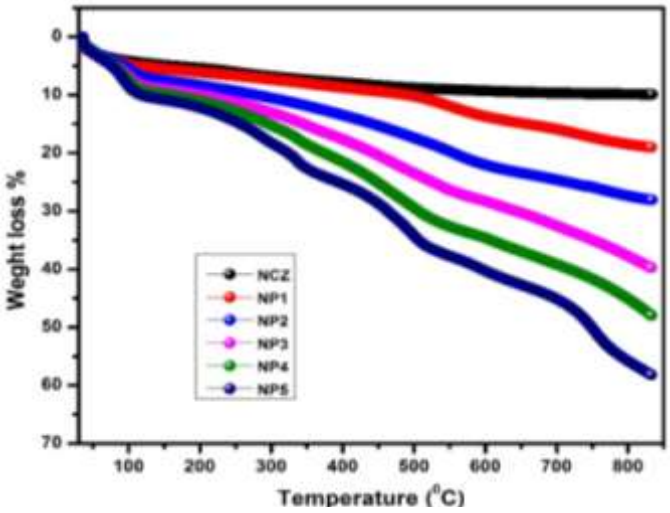

Figure 5: TGA graphs for NCZ-PANI nanocomposites. Reproduced with permission from, Raju, P., A. Thirupathi, Ch Kalyani, Sk Mahammed Ali, J. Shankar, G. Neeraja Rani, J. Anjaiah, and M. Kanaka Durga. "Synthesis and thermal stability of ferrites added polymers nanocomposites." Materials Today: Proceedings (2023).

Figure 6 shows a graph that shows the direct current (dc) conductivity in NCZ-PANI nanocomposites at room temperature as a function of the weight % of PANI. According to the graph, conductivity diminishes as NCZ concentration rises. This behaviour is probably caused by interactions between the polymer and NCZ nanoparticles, which raise resistivity and, as NCZ concentration rises, decrease conductivity of NCZ-PANI nanocomposites by increasing dispersion of charge carriers [36, 37]. This behaviour may also be influenced by other elements, such as enhanced charge carrier trapping, which may be brought on by the nanoparticles themselves or by induced morphological alterations and defects. We suggest that the oxidation of polyaniline molecules results in the creation of polarons, which would explain the conductivity of our samples. Bipolarons, which are doubly charged defects that are delocalized over many rings of polyaniline, may be produced when these polarons unite to make them.

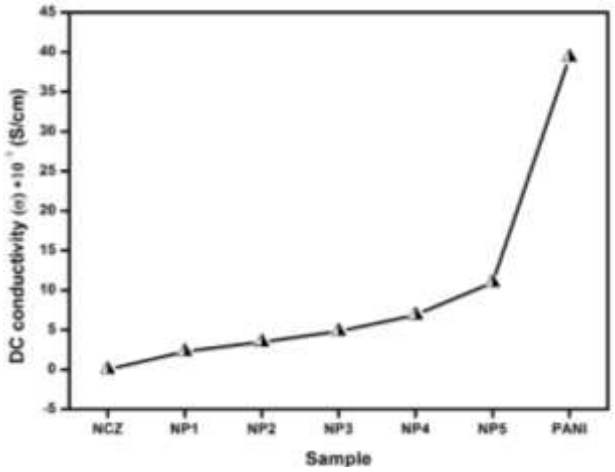

Figure 6: DC conductivity of NCZ-PANI nanocomposites at room temperature. Reproduced with permission from, Raju, P., A. Thirupathi, Ch Kalyani, Sk Mahammed Ali, J. Shankar, G. Neeraja Rani, J. Anjaiah, and M. Kanaka Durga. "Synthesis and thermal stability of ferrites added polymers nanocomposites." Materials Today: Proceedings (2023).

1. **Complex permittivity spectra of NCZ-PANI nanocomposites:** Figures 7 show the real and hypothetical parts of the complex permittivity spectra (ε*) for NCZ-PANI nanocomposites in the X-band (8–12 GHz). The NCZ value is quite low at 6.87 at 8.2 GHz, and it behaves almost consistently across the frequency range with the exception of a resonance peak at 9.7 GHz. It was found that when the weight % of PANI rose, both the real (ε') and imaginary component (ε") of the permittivity increased.

   Real permittivity is mostly dependent on interfacial polarizations between ferrite nanoparticles and polyaniline nanofibers as well as polarizations inside the polymer structure. Conducting polyaniline in its emeraldine base form may be protonated to produce persistent electric dipoles. The process of dielectric polarisation in ferrites is similar to that of electrical conduction, and NCZ is a ferrimagnetic material with high resistance. Thus, the collective behaviour of both types of electric charge carriers, electrons and holes, may be linked to the change in dielectric permittivity. Rezlescue's model [38] can be used to describe this occurrence. can be used to describe this occurrence. Electric conduction and dielectric polarisation in ferrites are supposedly caused by electron exchange between Fe2+ and Fe3+ ions and hole transfer between the substituted metallic ions [39, 40]. As a result, orientation (dipolar) polarisation predominates in both situations, and the associated relaxation events serve as the loss mechanisms. Furthermore, the limited conductivity of polyaniline results in joule-heating loss. Interfacial polarisation becomes a substantial polarisation process when the polymer diminishes the system's homogeneity, resulting in a heterogeneous system, and it adds to relaxation and loss processes [41].

   Interfacial polarisation and orientational polarisation are anticipated to be the main sources of ε' in these composites. Lower ε' values are produced by a declining polyaniline content as well as a decreasing contribution from orientational polarisation. Naturally, both of the aforementioned contributions will be at their highest levels when the composite has an equal amount of conductor (polyaniline) and insulator (NCZ), resulting in the highest possible net polarisation in NP5. As seen in Fig. 7b, the values of ε" at all frequencies rise as the concentration of polyaniline rises. This is predicted since increasing polyaniline concentration increases both dc/ac conductivity and dipole relaxation. The complex permittivity values for each sample are shown in Table 4. In the case of samples NCZ, NP1, NP2, and NP3, the resonance peaks seen at 9.7 GHz may be attributed to ferrite relaxation events. Due to the increased conductive loss caused by the higher proportion of polyaniline and lower percentage of NCZ, this resonance may be hidden in the remaining composites (NP4, NP5).

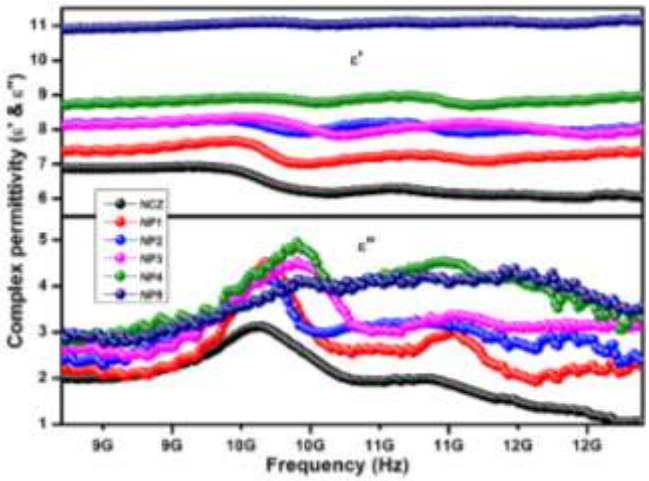

Figure 7: Complex permittivity of NCZ-PANI nanocomposites in X-band region. Reproduced with permission from, Raju, P., J. Shankar, J. Anjaiah, and S. R. Murthy. "Shielding effectiveness studies of NiCuZn ferrite-polyaniline nanocomposites for EMI suppression applications." In AIP Conference Proceedings, vol. 2162, no. 1. AIP Publishing, 2019.

In the Ku-band frequency range of 12–18 GHz, Figure 8 shows the complicated permittivity (ε*) spectra of NCZ and NCZ-PANI nanocomposites. The chart clearly shows that when PANI content rises, the values of ε' and ε" show a rising tendency. The increase in ε' can be attributed to the possibility that conductive PANI content in nanocomposites may grow, resulting to increased orientation polarisation and higher ε' values. Furthermore, there is a resonant behaviour in permittivity at about 15.5 GHz. Conductance resonance that takes place within and between nanoparticles is thought to be the cause of dielectric resonance in the Ku-band [42]. The details of ε' s and ε" values are exhibited in Table 4. The ε' value is shown to rise from 5.43 for NCZ to 9.02 for NP5, while ε" rises for NP5 from 1.003 for NCZ to 2.122.

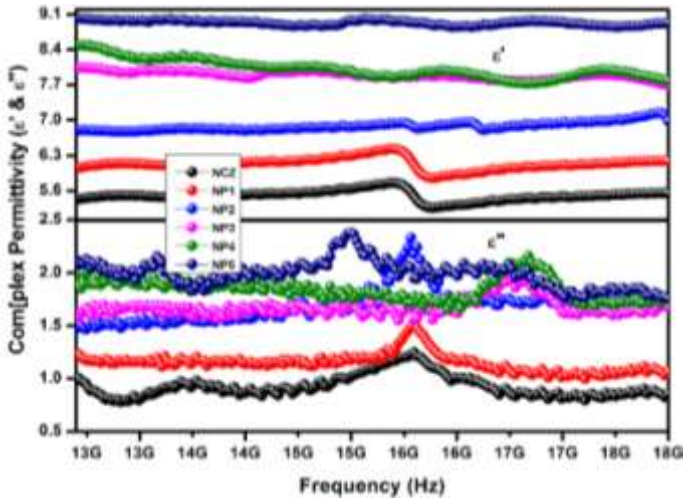

Figure 8: Complex permittivity of NCZ-PANI nanocomposites in the Ku-band region. Reproduced with permission from, Raju, P., J. Shankar, J. Anjaiah, and S. R. Murthy. "Shielding effectiveness studies of NiCuZn ferrite-polyaniline nanocomposites for EMI suppression applications." In AIP Conference Proceedings, vol. 2162, no. 1. AIP Publishing, 2019.

Understanding the dielectric loss, magnetic loss, and their interplay is crucial to comprehending microwave absorption characteristics. To further understand the underlying processes causing permittivity dispersion, we have used the Cole-Cole model, also known as the Debye dielectric relaxation model. Figure 9 (a–c) makes clear that the NCZ–PANI nanocomposites' full ε'-ε" curves display at least two Cole–Cole semicircles. This finding suggests that in addition to Debye relaxation, NCZ-PANI nanocomposites also exhibit Maxwell-Wagner relaxation, electron polarisation, and dipolar polarisation. Along with the Debye relaxation process, these new processes help the nanocomposites' improved dielectric characteristics. The existence of surfaces inside the nanocomposites causes interfacial polarisation or the Maxwell-Wagner effect. Due to charge buildup at interfaces and the development of significant dipoles on particles or clusters, this phenomenon develops in heterogeneous media [43]. The deformed Cole-Cole semicircle implies that, in addition to dielectric relaxation, other factors may also contribute to the permittivity spectra, such as conductance loss, interfacial polarisation, and the existence of oxygen defects [44].

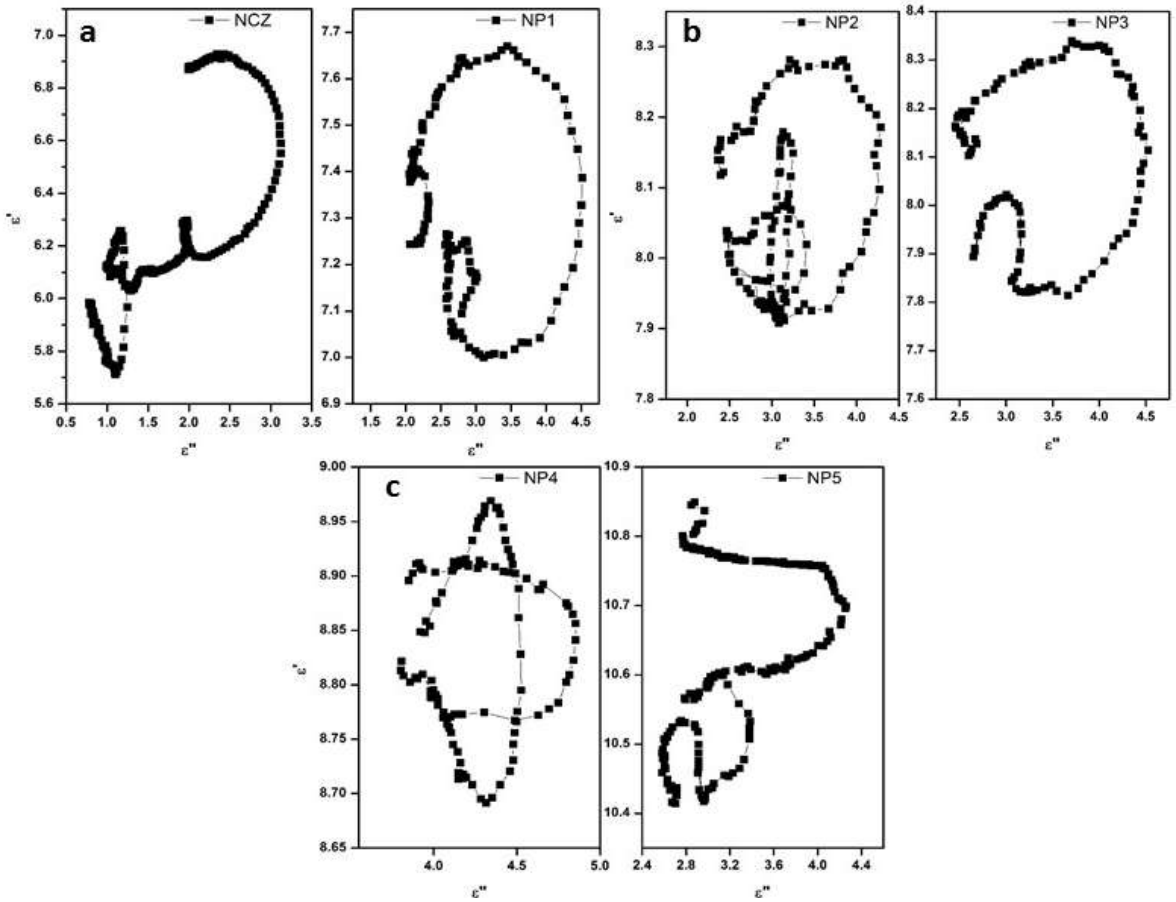

Figure 9: Typical Cole–Cole semicircles (ε′ versus ε″) for (a) NCZ & NP1, (b) NP2 &NP3 and (c) NP4 &NP5 in the frequency range of 8.2–18 GHz. Reproduced with permission from, Raju, P., P. Neelima, G. Neeraja Rani, and M. Kanakadurga. "Enhanced microwave absorption properties of Ni0. 48Cu0. 12Zn0. 4Fe2O4+ polyaniline nanocomposites." Journal of Physics and Chemistry of Solids 154 (2021): 110048.

- **Complex Permeability Spectra of NCZ-PANI Nanocomposites:** Figure 10 shows the real (μ′) and imaginary (μ″) components of NCZ-PANI nanocomposites' complex

permeability in the X-band (8–12 GHz) frequency range. The elastic or dispersion component, which is sometimes referred to as the actual part of complex permeability (μ′), reflects the magnetic energy held inside materials. The magnitude of magnetic energy dissipation within materials is depicted by the imaginary part (μ″), also known as the inelastic or absorption component. For the NCZ sample, the imaginary component (μ') shows a resonance peak at 10.5 GHz, whereas the real permeability part (μ') declines as the frequency rises from 8.2 to 12 GHz. With more polymer present, composites' real permeability (μ') decreases. When magnetic materials are coated with non-magnetic materials or mixed with them, a decrease in permeability is frequently noticed. It has been suggested that this is because of the decrease in saturation magnetization that occurred after their contact with nonmagnetic materials [45].

Eddy currents, natural resonances, and anisotropy energy inherent in the composites all contribute to the magnetic loss (μ") [46]. The inclusion of nano-sized ferrite particles in the composite mostly causes eddy current effects in the microwave frequency band. The tiny size of the ferrite particles in the composites is thought to be responsible for the natural resonances in the X-band. Small-sized materials have increased anisotropy energy at the nanoscale, especially because of the surface anisotropic field brought on by the small-size effect [48]. The greater microwave absorption is also a result of the higher anisotropy energy. With regards to μ", prominent resonance peaks are perceptible for the composite samples at about 10 GHz. High-frequency resonance peaks in the'curve are connected to exchange resonance, whereas lower-frequency peaks are connected to natural ferromagnetic resonance, according to Aharoni's hypothesis [49] [50]. The magnetic loss rises together with the polymer concentration. This rise might be explained by the magnetic loss in pure ferrite and composite materials, which is caused by a synergistic interaction between high-frequency natural resonance and domain wall resonance.

Table 4: lists the complex permeability values for NCZ-PANI nanocomposites

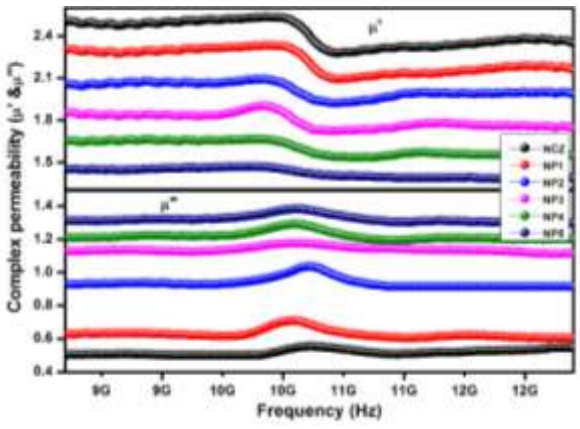

Figure 10: Complex permeability of NCZ-PANI nanocomposites in X-band region. Reproduced with permission from, Raju, P., J. Shankar, J. Anjaiah, and S. R. Murthy. "Shielding effectiveness studies of NiCuZn ferrite-polyaniline nanocomposites for EMI suppression applications." In AIP Conference Proceedings, vol. 2162, no. 1. AIP Publishing, 2019.

The complex permeability for nanocomposite samples (NCZ-PANI) measured in the Ku-band frequency range is shown in Figure 11 as the real (μ') and imaginary (μ") components (12-18 GHz). From the figure it is shown that the μ′ is decreased and μ″ is increased with increase in the addition of nonmagnetic PANI content in the sample. As the PANI concentration rises, Figure 5.6 shows that both μ' and μ" resonance peaks of the complex permeability move to higher frequencies. According to spin rotational resonance, a phenomena sensitive to composition and structure [51, 52], the resonance peaks, which appear between 14.5 and 17 GHz in the composites, are responsible. The values of' μ′ & μ″ for the nanocomposites at 12.4 GHz are shown in Table 4. With an increase in PANI content, the'value falls from 2.35 to 1.35 while μ" rises from 0.501 to 1.299.

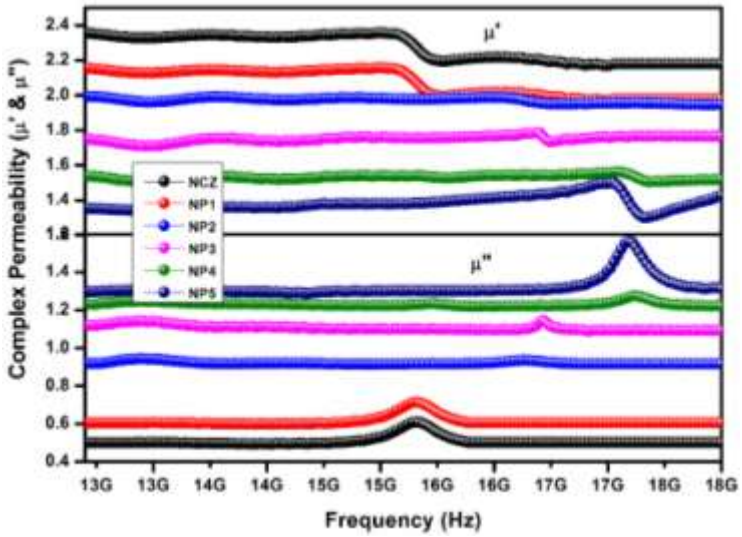

Figure 11: Complex permeability of NCZ-PANI nanocomposites in the Ku-band region. Reproduced with permission from, Raju, P., J. Shankar, J. Anjaiah, and S. R. Murthy. "Shielding effectiveness studies of NiCuZn ferrite-polyaniline nanocomposites for EMI suppression applications." In AIP Conference Proceedings, vol. 2162, no. 1. AIP Publishing, 2019.

Table 4: Complex permittivity properties of NCZ-PANI nanocomposites. Reproduced with permission from, Raju, P., J. Shankar, J. Anjaiah, and S. R. Murthy. "Shielding effectiveness studies of NiCuZn ferrite-polyaniline nanocomposites for EMI suppression applications." In AIP Conference Proceedings, vol. 2162, no. 1. AIP Publishing, 2019.

S. No	Sample code	Conductivity S/cm	at 8.2 GHz (X-band)				at 12.4 GHz (Ku-band)			
			ε'	ε"	μ'	μ"	ε'	ε"	μ'	μ"
1	NCZ	$1.13*10^{-6}$	6.80	2.012	2.52	0.504	5.43	1.003	2.35	0.501
2	NP1	2.259*10-3	7.36	2.176	2.31	0.627	6.05	1.230	2.15	0.605
3	NP2	$3.475*10^{-3}$	8.12	2.430	2.05	0.929	6.79	1.470	1.99	0.918
4	NP3	$4.821*10^{-3}$	8.11	2.619	1.85	1.125	8.04	1.629	1.75	1.122
5	NP4	$6.874*10^{-3}$	8.70	2.849	1.65	1.211	8.48	1.969	1.54	1.232
6	NP5	$1.095*10^{-2}$	10.9	3.007	1.45	1.313	9.02	2.122	1.35	1.299

Due to the magnetic characteristics of the NCZ particles, the magnetic loss seen in NCZ-PANI nanocomposites greatly contributes to increasing microwave absorption. Hysteresis loss, eddy current loss, domain wall resonance, and natural resonance processes are the principal causes of this magnetic loss in magnetic materials such as ferrites [53, 54]. In the microwave spectrum, frequencies below 100 MHz, which are inconsequential, are where domain wall resonance generally occurs. The modest magnetic fields associated with microwaves do not experience hysteresis loss, but extremely strong external magnetic fields do. Eddy current loss and natural resonance loss are thus the main elements affecting magnetic loss in the microwave frequency range [55]. The eddy current effect frequently has an impact on the microwave absorption characteristics of ferrite composite absorbers in the high-frequency range. The mathematical representation of the parameter is [56].

$$\mu'' \approx 2\pi\mu_0(\mu')^2\sigma \cdot d^2 f/3 \qquad \text{-- (4)}$$

where σ and μ0 are the electric conductivity and the permeability in vacuum, respectively. Thus, C0 can be described by

$$C_0 = \mu''(\mu')^{-2} f^{-1} = 2\pi\mu_0\sigma \cdot d^2/3 \qquad \text{-- (5)}$$

If the magnetic loss results from eddy current loss, the values of C0 are constant when the frequency is varied which is called the skin-effect criterion. [57, 58]

The Cole-Cole plots for the NCZ-PANI nanocomposites are shown in Figures 12a to 12c. These plots show semicircular or elliptical-shaped curves that represent relaxation dispersion, which is defined by variations in μ′ versus μ″. These curves differ in form from the normalised curve of μ* [59], even though they reflect relaxation events. Due to damping in the magnetization process, NiCuZn ferrites and other spinel ferrites exhibit relaxation phenomena more frequently in a variety of applications. As PANI concentration rises, the Cole-Cole plots reveal a tendency for a smaller ellipsoid curve, which results in narrower peaks in μ*, as seen in Figure 5. This form variation provides a distinct way to illustrate relaxation processes in various ferrites.

The C0-f curves of pure NCZ and NCZ-PANI nanocomposites are shown in Figure 12d. In the high-frequency band, C0 values are essentially constant for pure NCZ (8-18 GHz). While pure NCZ has a large eddy current effect in the high-frequency range (8.2-18 GHz), which decreases with the addition of PANI, NCZ-PANI nanocomposites show two resonance peaks in the studied frequency range. Furthermore, eddy current effects and natural resonance are the main causes of magnetic loss in NCZ-PANI nanocomposites.

Natural resonance has the following relationships between the resonance frequency (fr) and the anisotropy field (Ha): Where is the gyromagnetic ratio, the formula is 2πfr = γHa. (γ is the gyromagnetic ratio) Additionally, Ha is proportional to the magnetic crystal's anisotropy constant (K1), using the formula Ha = 4|K1|/3 0Ms. For cubic NCZ ferrite, the anisotropy constant K1 is 1.1 x 104 J/m3. As a result,

the intrinsic resonance frequency (fr) in bulk magnetic materials is usually in the hundreds of Hz range. However, the nanometer size effect dramatically affects Ha at the particle surface for magnetic particles that are nanoscale in size, causing a large rise. The resonant frequencies (fr) of this phenomenon may reach the GHz range. Thus, natural resonance loss resulting from nanosized magnetic nanoparticles contributes to the magnetic loss seen in nanocomposites in the X-band.

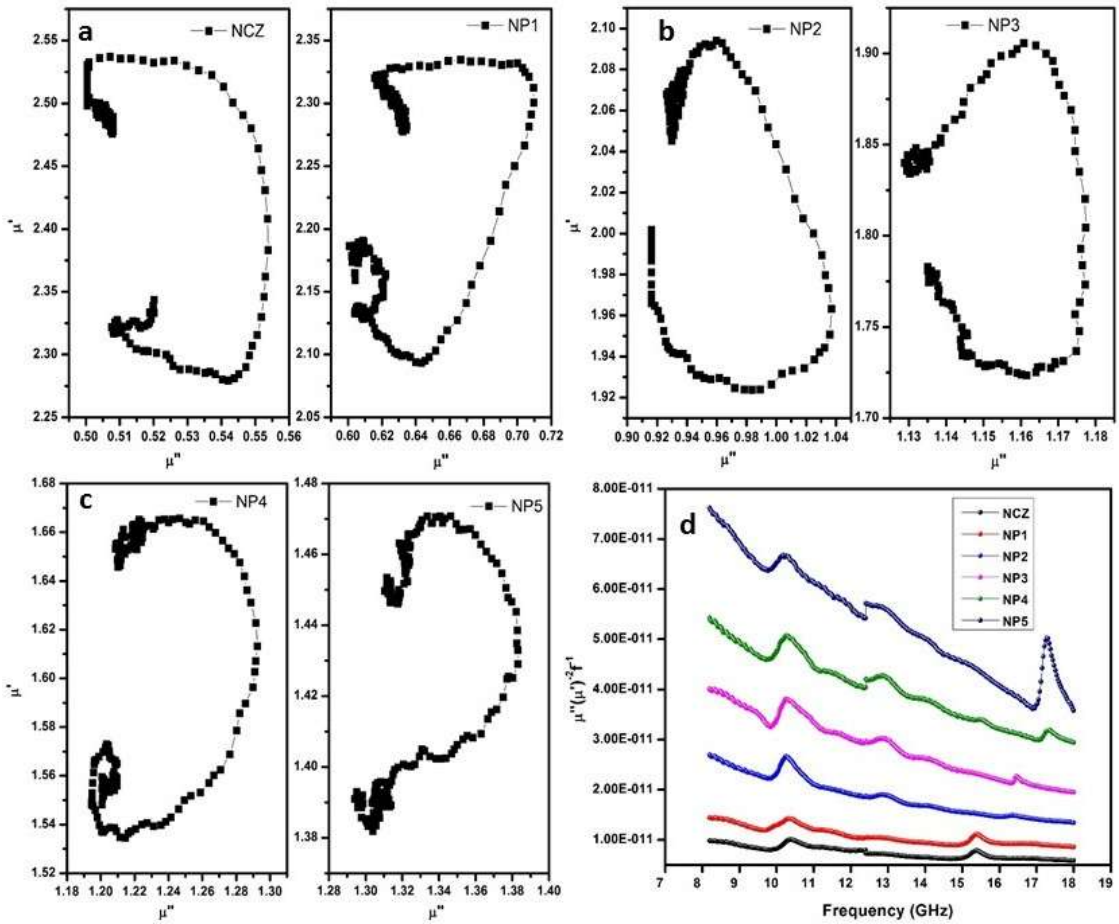

Figure 12 (a-c) cole-cole plot of complex permeability of a) NCZ, NP1 b) NP2, NP3 c) NP4, NP5 d) Plot of $\mu''(\mu')^{-2}f^{-1}$ vs. frequency for the NCZ-PANI nanocomposite. Reproduced with permission from, Raju, P., P. Neelima, G. Neeraja Rani, and M. Kanakadurga. "Enhanced microwave absorption properties of Ni0. 48Cu0. 12Zn0. 4Fe2O4+ polyaniline nanocomposites." Journal of Physics and Chemistry of Solids 154 (2021): 110048.

The S-parameters are related to the voltage of the reflected (R) and incident (I) waves and can be correlated with the respective powers (P) by:

$$P_R = |S_{11}|^2 = |S_{22}|^2 \quad (6)$$
$$P_T = |S_{12}|^2 = |S_{21}|^2 \quad (7)$$

Thus, the absorbed power (PA) can be calculated taking into account that the incident power (P_I) is 1 mW as:

$$P_A = 1 - P_R - P_T = 1 - |S_{11}|^2 = |S_{12}|^2 \quad (8)$$

To reflect the loss of incident power, as the wave strikes the material and passes through it, the S-parameters can be conveniently assessed to obtain the total shielding efficiency and to separate the absorption and reflection loss contributions as:

$$SE_T = -10\log\frac{P_I}{P_T} = SE_R(dB) + SE_A(dB) = -10\log\frac{1}{|S_{21}|^2} \quad (9)$$

$$SE_R = -10\log\frac{P_I}{P_I - P_R} = -10\log\frac{1}{1-|S_{11}|^2} \quad (10)$$

$$SE_A = -10\log\frac{P_I - P_R}{P_T} = -10\log\frac{1-|S_{11}|^2}{|S_{21}|^2} \quad (11)$$

The reflection coefficient, Transmission coefficient, Absorption coefficient, Absorption efficiency and Shielding effectiveness were calculated using equations 6-11.

Figures 13 and 14 show the variations in the values of the reflection, transmission, and absorption coefficients for NCZ-PANI nanocomposites positioned within rectangular waveguide cross-sections at various frequencies. The reflection coefficient increases with increasing polymer content in the nanocomposites across the whole frequency range. This shows that increasing polymer content in nanocomposites causes larger magnitudes of reflection coefficients and lower magnitudes of transmission coefficients. As a result, samples with higher polymer content show increased reflection and lower transmission.

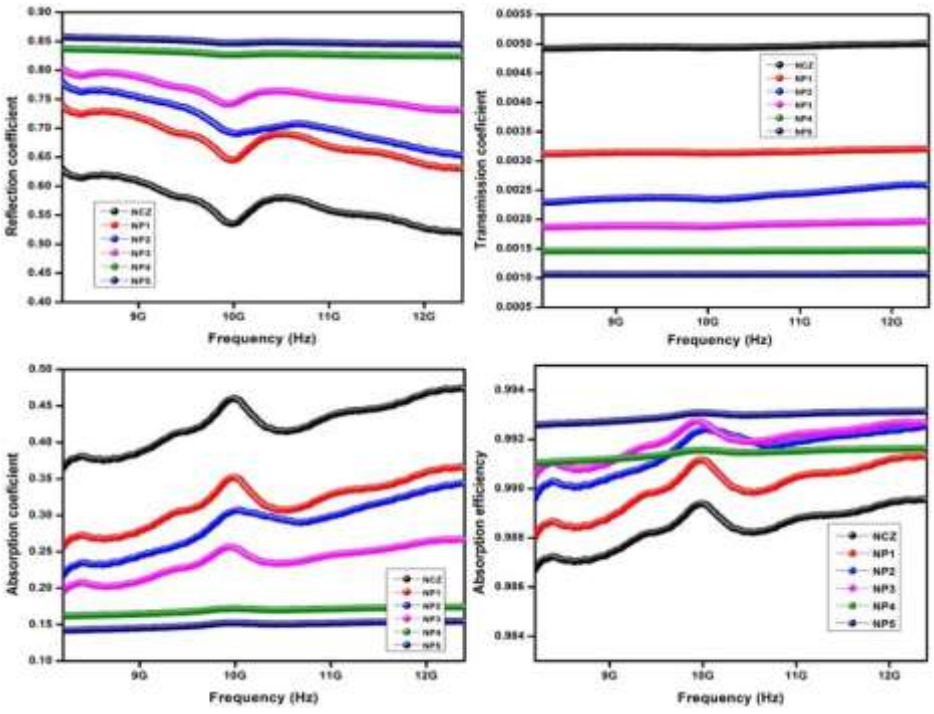

Figure 13: Reflection, Transmission, Absorption coefficients and Absorption efficiency of NCZ-PANI nanocomposites in X band region.

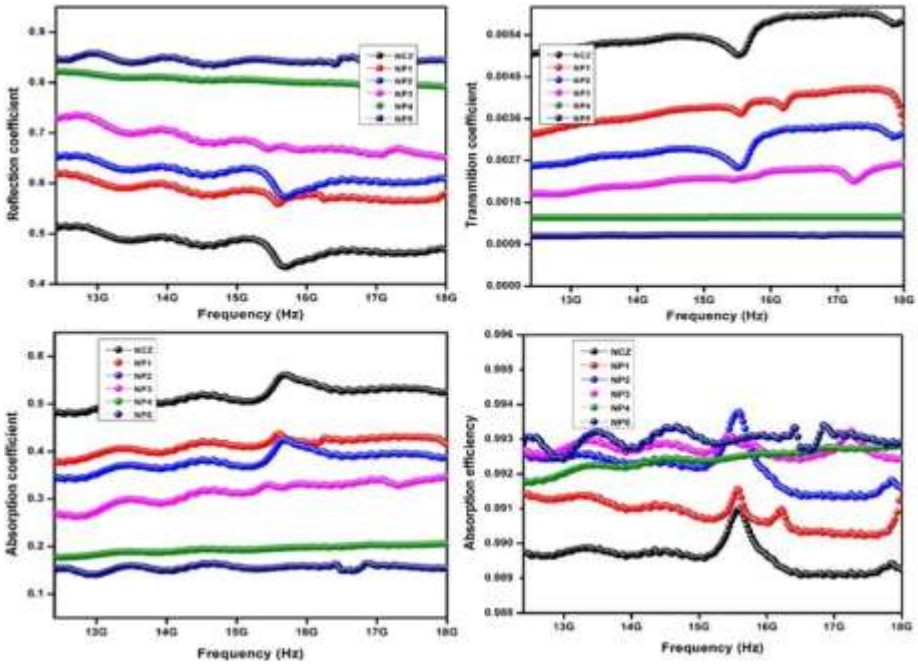

Figure 14: Reflection, Transmission, Absorption coefficients and Absorption efficiency of NCZ-PANI nanocomposites in Ku band region.

Figures 15(a & b) and 16 show the electromagnetic interference (EMI) shielding efficacy for NCZ-PANI nanocomposites in terms of reflection (SER), absorption (SEA), and total shielding effectiveness (SET). Between NCZ and NP5, the overall shielding efficacy has significantly enhanced, rising from 23.08 dB to 29.75 dB. With a maximum of 21.47 dB found for sample NP5, Table 5's detailed figures show that absorption is the main factor that affects shielding effectiveness (SE) in the NCZ-PANI nanocomposite. SEA grows together with the proportion of conducting polymer. On the other hand, with SER values ranging from 4.32 dB to 8.45 dB, the shielding efficacy attributable to reflection is still rather modest. Higher polymer content in the composites results in increased SE and outstanding stability across the studied frequency range. The enhanced dielectric and magnetic losses in the polymer composites can be blamed for this increased absorption with the addition of PANI. The increased conductivity and dielectric constant of the nanocomposites, which support their high EMI shielding effectiveness, can also be used to explain it.

The primary method of EMI shielding is the reflection of incoming electromagnetic radiation off the shield. The interaction between the free electrons present on the conducting shield's surface and the EMI radiation is what causes this. Even though it is less noticeable, EMI shielding by absorption includes electromagnetic waves interacting with electric dipoles in the shield material. Conducting substances, such conducting polymers and carbon nanotubes, primarily protect EMI by reflection rather than absorption.

The fundamental principle of EMI shielding states that the best microwave shield should be a multiphase composite that has the right amounts of magnetic material, dielectric filler, and electrically conducting material. The shield's physical

shape is also extremely important for improving shielding efficacy. By enabling reflection off the conducting shield's front face as a result of interactions with mobile charge carriers and ohmic losses, moderate conductivity in the range of 10-4 to 10-1 S/cm enhances SE (heat). In addition, space charge polarisation is present in materials with a lot of charge carriers, which heightens the polarisation effect.

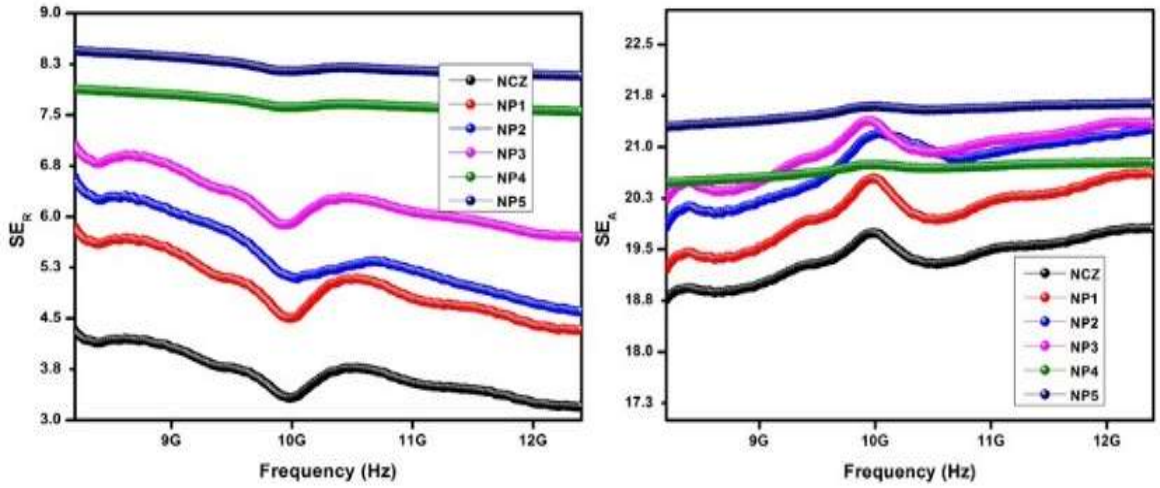

Figure 15: EMI shielding effectiveness a) due to Reflection (SE_R) and b) due to Absorption of NCZ–PANI nanocomposites in X-band region. Reproduced with permission from, Raju, P., J. Shankar, J. Anjaiah, and S. R. Murthy. "Shielding effectiveness studies of NiCuZn ferrite-polyaniline nanocomposites for EMI suppression applications." In AIP Conference Proceedings, vol. 2162, no. 1. AIP Publishing, 2019.

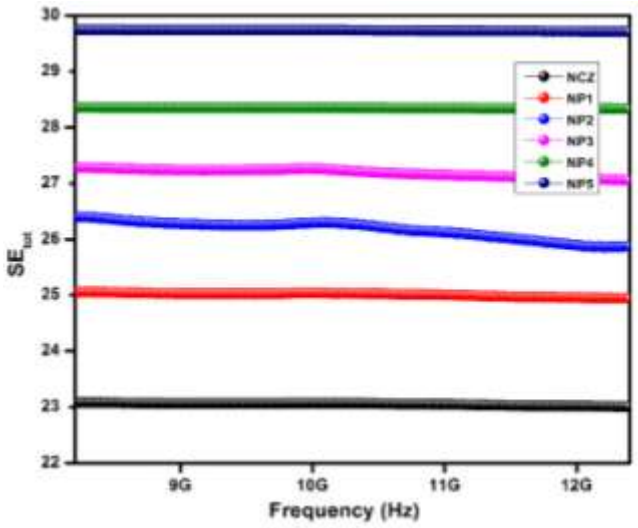

Figure 16: EMI Total shielding effectiveness (SE_{tot}) of NCZ–PANI nanocomposites in X-band region. Reproduced with permission from, Raju, P., J. Shankar, J. Anjaiah, and S. R. Murthy. "Shielding effectiveness studies of NiCuZn ferrite-polyaniline nanocomposites for EMI suppression applications." In AIP Conference Proceedings, vol. 2162, no. 1. AIP Publishing, 2019.

Figures 17(a & b) and 18 show the EMI shielding efficiency (SE) of NCZ-PANI nanocomposites in the Ku-band frequency range. These SE plots show an association between PANI frequency and weight ratio. The SE of the nanocomposites grows as PANI's weight ratio does. The SE values for CFF composites with 0, 10, 20, 30, 40, and 50 wt percent PANI, respectively, at 12.4 GHz are 23.03, 24.88, 25.92, 27.05, 28.32, and 29.71 dB. In general, variables including reflection off the material's surface, absorption of electromagnetic (EM) energy, and the pathways travelled by EM waves affect the EMI shielding performance of these composites. These elements depend on the filler's characteristics, forms, sizes, and microstructures.

The findings also comprise information on the efficiency of shielding owing to reflection (SER) and absorption (SEA), which is shown in Figures 17a and b. Notably, SEA values considerably rise over the whole frequency range when the weight ratio of PANI rises. The SEA values at 12.4 GHz are 19.87, 20.66, 21.28, 21.32, 20.82, and 21.47 dB for composites containing 0, 10, 20, 30, 40, and 50 wt percent PANI, respectively. However, the highest SER value for NCZ-PANI nanocomposites is 8.23 dB, and it tends to rise with increasing PANI concentration. It's important to note that the SEA values are invariably greater than the SER values, showing the NCZ-PANI composites' strong absorption properties with regard to EM wave interactions.

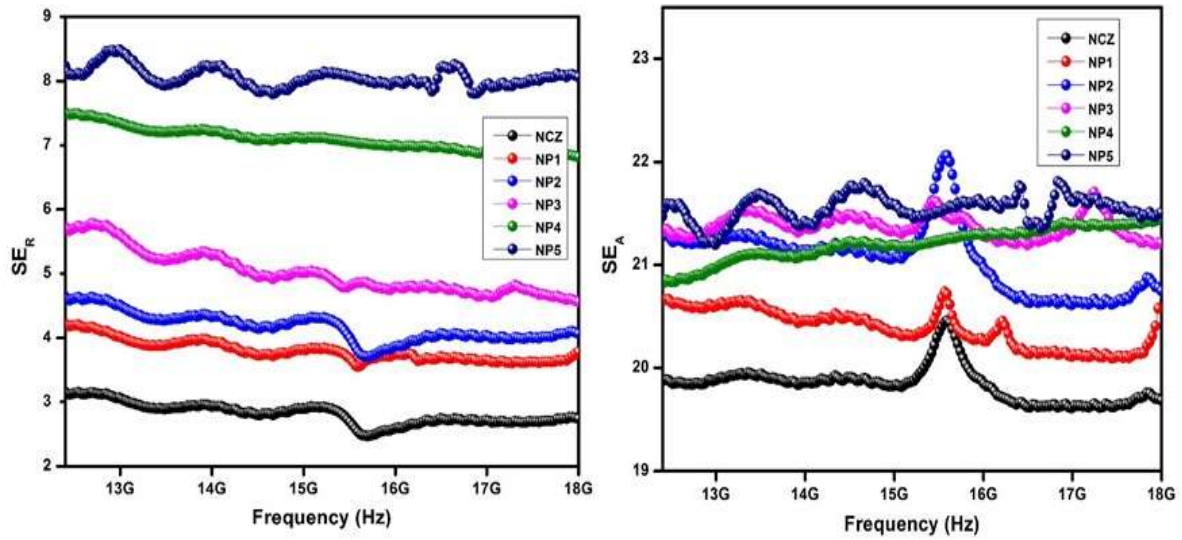

Figure 17: EMI shielding effectiveness a) due to Reflection (SE_R) and b) due to Absorption of NCZ–PANI nanocomposites in Ku-band region. Reproduced with permission from, Raju, P., J. Shankar, J. Anjaiah, and S. R. Murthy. "Shielding effectiveness studies of NiCuZn ferrite-polyaniline nanocomposites for EMI suppression applications." In AIP Conference Proceedings, vol. 2162, no. 1. AIP Publishing, 2019.

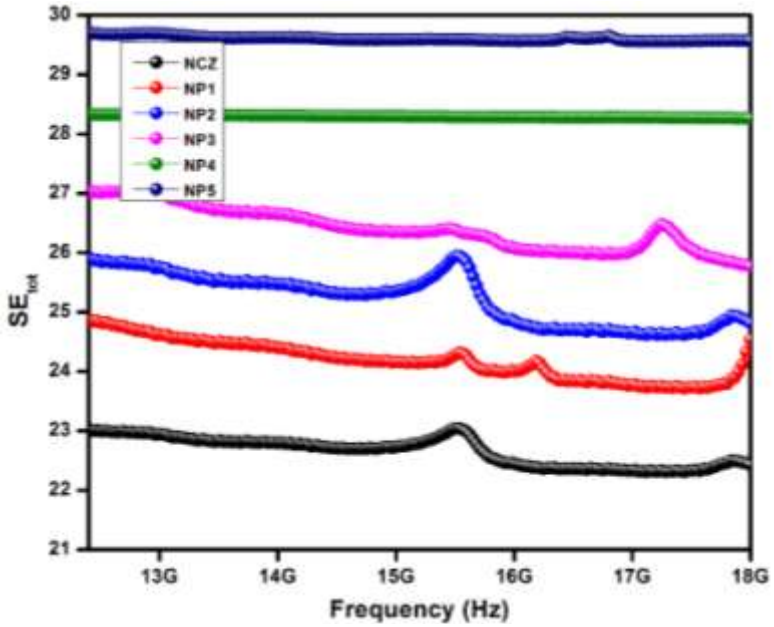

Figure 18: EMI Total shielding effectiveness (SE_{tot}) of NCZ–PANI nanocomposites in Ku-band region. Reproduced with permission from, Raju, P., J. Shankar, J. Anjaiah, and S. R. Murthy. "Shielding effectiveness studies of NiCuZn ferrite-polyaniline nanocomposites for EMI suppression applications." In AIP Conference Proceedings, vol. 2162, no. 1. AIP Publishing, 2019.

Table 5: Shielding effectiveness properties of NCZ-PANI nanocomposites. Reproduced with permission from, Raju, P., J. Shankar, J. Anjaiah, and S. R. Murthy. "Shielding effectiveness studies of NiCuZn ferrite-polyaniline nanocomposites for EMI suppression applications." In AIP Conference Proceedings, vol. 2162, no. 1. AIP Publishing, 2019.

S. No	Sample code	at 8.2 GHz (X-band)			at 12.4 GHz (Ku-band)		
		SE_R	SE_A	SE_{tot}	SE_R	SE_A	SE_{tot}
1	**NCZ**	4.32	18.76	23.08	3.15	19.87	23.03
2	**NP1**	5.85	19.20	25.06	4.22	20.66	24.88
3	**NP2**	6.57	19.83	26.40	4.64	21.28	25.92
4	**NP3**	7.05	20.22	27.28	5.73	21.32	27.05
5	**NP4**	7.88	20.47	28.36	7.50	20.82	28.32
6	**NP5**	8.45	21.29	29.75	8.23	21.47	29.71

Reflection loss (RL), a crucial factor that measures a material's capacity to absorb microwaves, is measured in decibels (dB). If there is no transmitted energy and the reflection coefficient reaches a value of -10 dB, the microwave absorber will have absorbed 90% of the incoming energy. Another significant aspect of microwave absorbers is their operating frequency range, which is calculated as the difference between the maximum (fmax) and lower (fmin) frequencies at which RL is still less than -10 dB.

We investigate the reflection loss (RL) in these materials in order to forecast their microwave absorption capability. Generally speaking, materials with higher negative RL values have better microwave absorption characteristics. The interaction between electromagnetic-absorbing materials' complicated permittivity and permeability determines how well they absorb microwaves in most cases. To maintain electromagnetic compatibility, it is frequently necessary to balance magnetic loss with dielectric loss in order to achieve optimal microwave absorption.

The RL value measures the microwave absorption capacity of a substance. The complex permittivity and complex permeability observed values are employed in a model based on a single-layered plane wave absorber presented by Naito and Suetake [72] to determine the RL. The wave impedance (Z) at the air-absorber interface is specified as follows in this model:

$$Z_{in} = Z_0 \left(\frac{\mu^*}{\varepsilon^*}\right)^{1/2} \tanh\left\{j\left(\frac{2\pi f d}{c}\right)(\mu^*\varepsilon^*)^{1/2}\right\} \quad \text{-- (12)}$$

where μ*=μ′-jμ″ and ε*=ε′-jε″ are the relative complex permeability and permittivity of the absorber medium, respectively. Zo=377 Ω and f are wave impedance and frequency, respectively, in free space, c is the velocity of light and d is the sample thickness.

The reflection loss (RL) in decibels (dB) is then determined as

$$RL = -20\log\left|\frac{Z_{in}-Z_0}{Z_{in}+Z_0}\right| \quad \text{-- (13)}$$

The impedance matching condition representing the perfectly absorbing properties is given by Zin=Zo. This condition is satisfied at a particular matching thickness (tm) and a matching frequency (fm), where minimum reflection loss occurs. [73]

In order to enhance absorption, the condition of zero reflection is attained using two different methods. The goal of the first strategy is to "match characteristic impedance," or make the material's inherent impedance equal to that of empty space. The second method uses the "matched-wave-impedance" principle, in which the wave impedance at the metal-backed material's surface is the same as the inherent impedance of empty space. The second notion was used in this investigation.

It is critical to make sure that the input impedance (Zin) equals 1, which precludes reflection, in order to meet the zero-reflection criterion and achieve maximum absorption. This is best accomplished when the material displays || = ||. In this case, the performance of the electromagnetic wave-absorbing material increases linearly with thickness. The values of complex permeability and complex permittivity greatly vary in the frequency range of interest, therefore this ideal scenario is seldom reached in practise.

There are two more situations that occur with |||||. The lowest reflection loss for materials with inherent impedances larger than unity (|| > ||) occurs at a thickness of the material around half a wavelength. On the other hand, for materials with inherent impedances less than unity (|| ||), the lowest reflection loss occurs at a thickness of about a fourth of the material's wavelength. Ferrites often display electromagnetic properties of || || in the microwave frequency region, earning them the moniker "quarter-wavelength absorbers." When the thickness of the material, measured within the absorbing material, coincides with an odd multiple of one-quarter of the incoming wavelength and the material has the proper loss factor for that particular thickness, the minimal loss occurs. Equation 14 may be used to express this thickness (d), where c stands for the speed of light and f for the frequency of interest [74]:

$$d = \frac{c}{4f\sqrt{|\mu^*|\,|\varepsilon^*|,}} = \frac{\lambda}{4}\frac{1}{\sqrt{|\mu^*|\,|\varepsilon^*|}} \quad \text{-- (14)}$$

The reflection loss values of NCZ-PANI and NCZ-PFD nanocomposites at various sample thicknesses were examined in the study. Using vector network analyzers, the microwave absorption characteristics of nanocomposites with a 2.1 mm thickness were evaluated across the frequency range of 8.2-18 GHz.

The correlation between reflection loss and frequency for NCZ-PANI nanocomposites is shown in Fig. 19. Notably, the minimal reflection loss showed two different dips in the NP3, NP4, and NP5 samples whereas it showed just one drop in the NCZ, NP1, and NP2 data. Table 5.9 gives specific values for the minimal reflection loss and the accompanying frequencies. The figure also shows that higher minimum reflection loss results from increased PANI concentration.

With a minimum reflection loss of only -28.50 dB and a bandwidth below -10 dB of around 2.1 GHz, pure NiCuZn ferrite nanoparticles showed modest absorption characteristics. However, when PANI was combined with NCZ ferrite, the absorption characteristics of NCZ-PANI nanocomposites dramatically improved. With a bandwidth below -10 dB reaching 9.8 GHz, these nanocomposites attained a minimal reflection loss of up to -39.74 dB. The complementary actions of NCZ and PANI are responsible for this improvement in absorption characteristics. First off, PANI increases dielectric loss by creating a full conductive network thanks to its sizable specific surface area. Second, magnetic loss is increased by the evenly disseminated NCZ ferrite nanoparticles on the polymer's surface. Oscillating currents are produced by dielectric relaxation and dielectric polarisation resulting from interface charges when incoming electromagnetic waves interact with the nanocomposites. The NCZ nanoparticles act as multipole polarisation centres on the surface of the polymer, enhancing electronic polarisation inside the nanocomposites and controlling incident electromagnetic waves to promote powerful electromagnetic wave absorption. Last but not least, the presence of PANI improves Debye dipole relaxation, which makes it easier for conjugated electron clouds to move between PANI and NCZ by way of the chains of PANI molecules. The NCZ-PANI nanocomposites' ability to absorb electromagnetic waves is amplified by this tunnel effect. Furthermore, large dielectric and magnetic losses are required for effective absorption materials, as well as excellent matching properties, where the dielectric loss closely matches or is equal to

the magnetic loss. Such matching characteristics greatly contribute to improved microwave absorption properties.

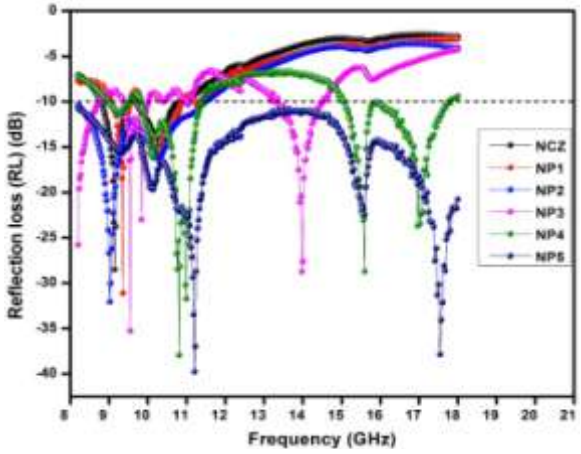

Figure 19: Reflection loss (RL) curves of NCZ-PANI nanocomposites

The frequency range across which the reflection loss remains below -10 dB is referred to as the "bandwidth" in this context. It indicates that the material has good potential for microwave applications when the reflection loss remains below this threshold across a broad frequency range. The NP5 sample, as seen in the image, has an absorption bandwidth that spans the whole frequency band range of 8.2-18 GHz. Due to its quality, it may be used for a wide range of purposes, such as military radar, satellite communications, accurate target identification, and direct broadcast satellites (DBS) for high-resolution images. The figures also clearly show that the bandwidth and reflection loss values increase as the PANI concentration in the nanocomposites rises. You can find specific values for reflection loss and bandwidth in Table 5.9 for all the nanocomposites studied.

It is interesting to note that the minimum reflection loss of present samples is significantly higher than those reported in the literature for comparable materials, i.e., PANI-NiZn-ferrite (-20 dB) [76], PANI-graphite-CoFe2O4 (-11.2 dB) [50 78], PANI-MnFe2O4 (-15.3 dB) [77], and PANI-BaFe12O19 (-19.7 dB) [84].

Table 6 Reflection loss values of NCZ-PANI nanocomposites in X-band region. Reproduced with permission from, Raju, P., P. Neelima, G. Neeraja Rani, and M. Kanakadurga. "Enhanced microwave absorption properties of Ni0. 48Cu0. 12Zn0. 4Fe2O4+ polyaniline nanocomposites." Journal of Physics and Chemistry of Solids 154 (2021): 110048.

S. No	Sample	Minimum reflection loss (dB) and frequency (GHz)	Bandwidth over −10 dB (GHz)
1	**NCZ**	-28.5 dB at 9.14 GHz	8.78-10.8
2	**NP1**	-31 dB at 9.35 GHz	9.06-10.86
3	**NP2**	-32 dB at 9.02 GHz	8.2-11.47
4	**NP3**	-35.26 at 9.29, -28.73 at 13.97	9.37-10.13, 13.38-14.53
5	**NP4**	-37.94 at 10.8, -28.7 at 15.59	8.99-11.39, 15.05-17.76
6	**NP5**	-39.74 at 11.2, -37.85 at 17.53	8.2-18

Fig. 20 shows the reflection losses of the NP5 nanocomposite at different matching thicknesses ranging from 0.5 mm to 4.5 mm in order to comprehensively study the appropriate thickness for the best microwave absorption performance. With a lowest reflection loss (RL) value of -42.10 dB at 9.35 GHz and a bandwidth of 4.2 GHz when the matching thickness is 2.5 mm, the NP5 nanocomposite demonstrates remarkable microwave-absorbing qualities, as shown in Fig. 5.16. Similarly, maximum reflection losses at 8.87 GHz, 11.95 GHz, and 12.51 GHz are respectively -39.43 dB, -39.21 dB, and -39.11 dB for matching thicknesses of 3.3 mm, 2.0 mm, and 2.2 mm. On the other hand, a matching thickness of 0.5 mm results in the lowest reflection loss at 18.0 GHz, which is -8.7 dB. At matching thicknesses of 4.0 mm and 4.5 mm, respectively, minimum reflection losses of -15.52 dB and -11.45 dB are noted.

It is obvious that the matching thickness plays a regulatory role, causing reflection loss peaks to shift towards lower frequencies as the matching thickness increases, according to the formula fm = C/2" dm, where fm stands for the frequency of the minimum reflection loss peak and dm is the matching thickness. This phenomena fits with the correlation between the thickness of the absorbent material (dm) and frequency (fm). It implies that the frequency fm and thickness dm of the absorbent material may both be changed to produce the best matching and absorption.

The lowest reflection loss of the nanocomposite first rises when the layer thickness is between 0.5 mm and 4.5 mm, as shown in Fig. 20, and subsequently lowers as the layer thickness rises. The minimal reflection loss values for various thicknesses are summarised in Table 7 in the table. The chart shows that, with a layer thickness of 2.5 mm, the lowest reflection loss has a bandwidth greater than -10 dB loss at 3.8 GHz and reaches its maximum value of -42.0 dB at 9.35 GHz. The greatest reflection loss starts to drop above a thickness of 2.5 mm, demonstrating that these wave-absorbing materials have a preferred thickness.

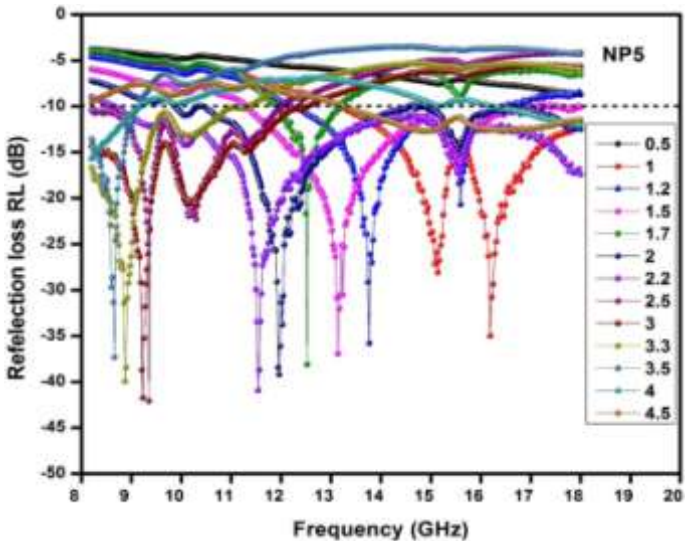

Figure 20: Reflection loss (RL) curves of NP5 sample for various thickness

Table 7: Reflection loss values of NP5 sample for different thicknesses

S. No	Sample thickness (mm)	Minimum reflection loss (dB) and frequency (GHz)	Bandwidth over −10 dB (GHz)
1	0.5	-8.7 dB at 18 GHz	--
2	1	-35.01 dB at 16.21 GHz	13.21-18
3	1.2	-35.79 dB at 13.76 GHz	12.21-16.49
4	1.5	-36.95 dB at 13.13 GHz	11.3-17.82
5	1.7	-39.11 dB at 12.51 GHz	11.91-13.16
6	2	-39.21 dB at 11.95 GHz	9.88-18
7	2.2	-40.92 dB at 11.53 GHz	8.66-18
8	2.5	-42.10 dB at 9.35 GHz	8.2-12
9	3	-41.74 dB at 9.22 GHz	8.2-12.4
10	3.3	-39.93 dB at 8.87 GHz	8.2-11.3
11	3.5	-37.31 dB at 8.66 GHz	8.2-9.12
12	4	-15.72 dB at 8.2 GHz	8.2-9.16, 16.24-18
13	4.5	-11.45 dB at 18 GHz	13.26-18

The NCZ-PANI and NCZ-PFD nanocomposites' reflection loss plots showed that the NP5 sample had the best microwave absorption performance, with a minimum reflection loss (RL) of -42.1 dB at a thickness of 2.5 mm and a frequency of 9.35 GHz. We've collated the reflection loss properties of several composite materials made of PANI and other magnetic particles that have been described in recent studies in Table 8. It is clear from the table that our present study's results perform better than those that have been reported in the literature. This demonstrates how well ferrite-polymer nanocomposites produce thin, strong materials for good microwave absorption applications. Notably, the NCZ-PANI nanocomposite (NP5) with a matching thickness of 2.1 mm greatly decreased the minimum reflection loss for pure ferrite from -28.49 dB (NCZ) to -39.74 dB. These results demonstrate how these materials can be used in the future as sophisticated microwave-absorbing materials.

Table 8: Microwave absorbing properties of different absorbers in previous references and this work

S. No	Absorber	Thickness (mm)	Minimum reflection loss and frequency	Bandwidth over −10 dB (GHz)	Ref
1	NiZn-ferrite-PANI	2.0	-20 dB at 14.0 GHz	12.1-16.7	76
2	$MnFe_2O_4$ -PANI	1.5	-15.3 dB at 10.4 GH	8.4-12.0	77
3	$CoFe_2O_4$ –PANI-graphite	2.0	-11.2 dB at 3.8GHz	3.4-4.1	78
4	Fe_3O_4 –PANI-CIP	2.0	-25.5 dB at 8.4 GH	7.1-10.0	79
5	Hollow PANI-Fe_3O_4 microsphere	2.0	-15.6 dB at 15.2 GHz	9.1-17.1	80
6	MnFe2O4 -Polypyrrole	1.5	−12 dB at 11.3 GHz	--	81
7	NiZnFe2O4	2.5	-24.5 dB at 8.5 GHz	7-11	82
8	SmSrFe2O4-PANI	3.0	-26.0 dB at 14.2 GHz	11.5-18	83
9	BaFe12O19-PANI	2.0	-17.8 dB at 9.5 GH	8.7-10.5	84
10	PANI-Fe3O4 microspheres	2.0	-18.6 dB at 14.0 GHz	12.1-16.0	85
11	NP5	2.1	-39.74 dB at 11.2 GHz -37.85 dB at 17.53 GHz	8.2-18	Present work

IV. CONCLUSIONS

In conclusion, we effectively created NCZ-PANI nanocomposites using mechanical milling. Through XRD, FT-IR, and SEM investigations, we looked at these composites' structural features. We also studied these nanocomposites electrically and magnetically. Our analysis of the frequency-dependent behaviour of the real and imaginary parts of permittivity and permeability in these nanocomposites showed that the presence of polymer increased complex permittivity while reducing the real and imaginary parts of permeability. Additionally, we looked at the X-band and Ku-band frequency ranges of the nanocomposites' frequency-dependent properties of reflection, transmission, absorption coefficients, and absorption efficiency. We discovered that the shielding efficacy values in NCZ-PANI nanocomposites improved with larger polymer content. Additionally, these nanocomposites attained an effective bandwidth (RL less than -10 dB) of 3.8 GHz, ranging from 8.2 to 12 GHz, and a minimum reflection loss of -41.72 dB at 9.35 GHz with a thickness of 3 mm, according to our tests of microwave absorption characteristics. An significant finding from our investigations is that when the PANI concentration rose, the nanocomposites' capacity for absorption increased while their density fell. This indicates that we used a lighter coating and yet got improved microwave absorption. Additionally, the nanocomposites' mechanical strength and flexibility were improved by the increased polymer content. The promise of NCZ-PANI nanocomposites as materials for microwave absorption applications is therefore quite high.

REFERENCES

[1] D.D.L. Chung, Carbon., 39 (2001) 279.
[2] Keyu Chen, Chen Xiang, Liangchao Li, Haisheng Qian, Qiushi Xiao and Feng Xu, J. Mater. Chem., 22 (2012) 6449
[3] R. D. C. Lima, M. S. Pinho, M. L. Gregori, C. ReisNunes and T. Ogasawara, Mater. Sci., 22 (2004) 245.
[4] M. J. Park, J. Choi and S. S. Kim, IEEE Trans. Magn., 36 (2000) 3272.
[5] V. Choudhary, Polym. Advn. Technol., 21 (2010) 1
[6] P. Saini, Synth. Met., 161 (2011) 1522,.
[7] F. F. Fang, B. M. Lee and H. J. Choi, Macromol. Res., 18 (2010) 99.
[8] P. Barber, S. Balasubramanian, Y. Anguchamy, S. Gong, A. Wibowo, H. Gao, H. J. Ploehn and H. Loye, Materials., 2 (2009) 1697.
[9] M. T. Sebastian and H. L. Jantunen, Int. J. Appl. Ceram. Technol., 434 (2010) 415.
[10] J. H. Jean, C. H. Lee, W. S. Kou, J. Am. Ceram. Soc. 82 (2) (1999) 343.
[11] R. Patil, A. S. Roy, K. R. Anilkumar, K. M. Jadhav and S. Ekhelikar, Composites, Part B., 43 (2012) 3406.
[12] Y. Li, H. Zhang, Y. Liu, Q. Wen and J. Li, Nanotechnology., 19 (2008) 105605.
[13] Y. Li, Y. Liu, J. Li, F. Long and J. Kang, J. Electron. Sci. Technol. Chin., 5 (2007) 296.
[14] Y. Li, H. Zhang, Y. Liu and J. Q. Xiao, Chin. J. Chem. Phys., 20 (2007) 739.
[15] P. Xiong, Q. Chen, M. He, X. Sun and X. Wang, J. Mater. Chem., 22 (2012) 17485.
[16] E. E. Tanrıverdi, A. T. Uzumcu, H. Kavas, A. Demir and A. Baykal, Nano-Micro Lett., 3 (2011) 99.
[17] S. Xuan, Y.-X. J. Wang, J. C. Yu and K. C.-F. Leung, Langmuir., 25 (2009) 11835.
[18] N. E. Kazantseva, Y. I. Bespyatykh, I. Sapurina, J. Stejskal, J. Vilˇ c´ akov´ a and P. S´ aha, J. Magn. Magn. Mater., 301 (2006) 155.
[19] O. Yavuz, M. K. Ram, M. Aldissi, P. Poddar and S. Hariharan, J. Mater. Chem., 15 (2005) 810.
[20] J. Jiang, L. Ai and L. C. Li, J. Mater. Sci., 44 (2009) 1025.
[21] X. Li, H. Yi, J. Zhang, J. Feng, F. Li, D. Xue, H. Zhang, Y. Peng and N. J. Mellors, J. Nanopart. Res., 15 (2013) 1.
[22] L. Li, P. Yih and D. Chung, J. Electron. Mater., 21 (1992) 1065
[23] V. Panwar, B. Kang, J.-O. Park, S. Park and R. Mehra, Eur. Polym. J., 45 (2009) 1777
[24] J.L. Guo, H. Wu, X.P. Liao, B.J. Shi, Journal of Physical Chemistry C., 115 (2011) 23688
[25] B. Assa, R. Nechache, D. Therriault, F. Rosei, M. Nedil, Applied Physics Letters 99 (2011) 183505.

[26] J. Jiang, L. Li, F. Xu, Journal of Physics and Chemistry of Solids., 68 (2007) 1656
[27] Ö. Yavuz, M. K. Ram, M. Aldissi, P. Poddar, S. Hariharan, Journal of Materials Chemistry 15 (2005) 810.
[28] K.W. Wagner, Ann. Phys., 40 (1993) 818.
[29] C.G. Koops, Phys. Rev., 83 (1951) 121.
[30] S. Xuan, Y.-X. J. Wang, J. C. Yu and K. C.-F. Leung, Langmuir., 25 (2009) 11835.
[31] S.K. Pradhan, S. Bid, M. Gateshki, V. Petkov, Mater. Chem. Phys., 93 (2005) 224.
[32] M.K. ElNimr, B.M Moharram, S.A Saafan, S.T Assar, J. Magn. Magn. Mater., 322 (2010) 2108
[33] E. C. Gomes and M. A. S. Oliveira, Am. J. Polym. Sci., 2 (2012) 7.
[34] A. H. Elsayed, M. S. M. Eldin, A. H. A. Elazm and H. A. Motaweh, Int. J. Electrochem. Sci., 6 (2011) 215.
[35] M. Gyu, Y. Jin, S. Woen and S. Soon, Synth. Mat., 124 (2001) 342.
[36] Z H Wang, H S Javadi, A Ray, A G Macdiarmid and A J Epstein, Phys. Rev., 42 (1990) 5411
[37] W Li and M Wan, Synth. Met., 92 (1998) 12
[38] N. Rezlescu, E. Rezlescu, Phys. Status Solidi A 23 (1974) 575.
[39] D. Ravinder, K. Latha, J. Appl. Phys. 75 (1994) 6118.
[40] A.M. Abdeen, J. Magn. Magn. Mater. 192 (1999) 121.
[41] Complex permittivity and microwave absorption properties of BaTiO3–polyaniline composite,. S.M. Abbas a,1, A.K. Dixit b, R. Chatterjee a,∗, T.C. Goel c,. Materials Science and Engineering B 123 (2005) 167–171
[42] K.J. Song, T. Pan, Q. Xue, Compact ultra-wideband notch-band bandpass filters using multiple slotline resonators, Microwave and Optical Technology Letters 54 (2012) 1132–1135.
[43] S. He, G. S. Wang, C. Lu, J. Liu, B. W., H. Liu, L. Guo and M. S. Cao, J. Mater. Chem. A., 1 (2013) 4685
[44] H. J. Wu, L. D. Wang, S. L. Guo, Y. M. Wang and Z.Y. Shen, Mater. Chem. Phys., 133 (2012) 965
[45] One-pot synthesis of CoFe2O4/graphene oxide hybrids and their conversion into FeCo/grapheme hybrids for lightweight and highly efficient microwave absorber Xinghua Li,‡ab Juan Feng,‡b Yaping Du,c Jintao Bai,a Haiming Fan,*ad Haoli Zhang,e Yong Peng*b and Fashen Lib,.. J. Mater. Chem. A, 2015, 3, 5535
[46] Conducting ferrofluid: a high-performance microwave shielding material,. Monika Mishra,a Avanish Pratap Singh,a B. P. Singh,b V. N. Singhc and S. K. Dhawan*a J. Mater. Chem. A, 2014, 2, 13159
[47] D. L. Leslie-Pelecky and R. D. Rieke, Chem. Mater., 1996, 8, 1770–1783.
[48] Y.-J. Chen, P. Gao, R.-X. Wang, C.-L. Zhu, L.-J. Wang, M.-S. Cao and H.-B. Jin, J. Phys. Chem. C, 2009, 113, 10061–10064.
[49] G. Viau, F. Fievet-Vincent, F. Fievet, P. Toneguzzo, F. Ravel and O. Acher, J. Appl. Phys., 1997, 81, 2749.
[50] F. S. Wen, F. Zhang and Z. Y. Liu, J. Phys. Chem. C, 2011, 115, 14025–14030.
[51] J. Xie, M. Han, L. Chen, R. Kuang and L. Deng, J. Magn. Magn. Mater., 2007, 314, 37.
[52] H. J. Kwon, J. Y. Shin and J. H. Oh, J. Appl. Phys., 1994, 75, 6109.
[53] X. Zhang, X. Dong, H. Huang, Y. Liu, W. Wang, X. Zhu, B. Lv, J. Lei and C. Lee, Appl. Phys. Lett., 89 (2006) 053115
[54] V. Petrov and V. Gagulin, Inorg. Mater. 37 (2001) 93.
[55] Jiacheng Wang, Hu Zhou, Jiandong Zhuang and Qian Liu, Phys.Chem.Chem.Phys., 17 (2015) 3802
[56] C. L. Zhu, M. L. Zhang, Y. J. Qiao, G. Xiao, F. Zhang, and Y. J. Chen, J. Phys. Chem. C., 114 (2010) 16229
[57] M. Z. Wu, Y. D. Zhang, S. Hui, T. D. Xiao, S. H. Ge, W. A. Hines, J. T. Budnick and G. W. Taylor, Appl. Phys. Lett., 80 (2002) 4404.
[58] X. F. Zhang, X. L. Dong, H. Huang, Y. Y. Liu, W. N. Wang, X. G. Zhu, B. Lv and J. P. Lei, Appl. Phys. Lett., 89 (2006) 053115.
[59] J. Smit and H. M. J. Wijn, Ferrites (Netherlands: Eindhoven) 78 (1959).
[60] Ohlan, A., et al., Microwave absorption properties of conducting polymer composite with barium ferrite nanoparticles in 12.4-18 GHz. Applied Physics Letters, 2008. 93(5).
[61] D. D. L. Chung, Carbon, 2001, 39, 279–285.
[62] Y. Yang, M. C. Gupta, K. L. Dudley and R. W. Lawrence, Nano Lett., 2005, 5, 2131–2134.
[63] R. C. Che, L. M. Peng, X. F. Duan, Q. Chen and X. L. Liang, Adv. Mater., 2004, 16, 401–405.
[64] P. Sambyal, A. P. Singh, M. Verma, M. Farukh, B. P. Singh and S. K. Dhawan, RSC Adv., 2014, 4, 12614–12624.
[65] Sambyal, P.; Singh, A. P.; Verma, M.; Farukh, M.; Singh, B. P.; Dhawan, S. K.;RSC Advances, 2014, 4 (24), 12614-12624. DOI: 10.1039/C3RA46479B
[66] Singh, A. P.; Mishra, M.; Sambyal, P.; Gupta, B. K.; Singh, B. P.; Chandra, A.; Dhawan, S. K.;Journal of Materials Chemistry A, 2014, 2 (10), 3581-3593. DOI: 10.1039/C3TA14212D

[67] Ebrahimi, F.; Nanocomposites - New Trends and Development., InTech: 2012.
[68] Das, C. K.; Mandal, A.;Nanocomposites., 2012, 1 (1), 43-53. DOI: 10.5539/jmsr.v1n1p45
[69] R13375–R13378, 1998.
[70] A. P. Singh, M. Mishra, P. Sambyal, B. K. Gupta, B. P. Singh, A. Chandra and S. K. Dhawan, J. Mater. Chem. A, 2014, 2, 3581–3593.
[71] B. Wen, X. X. Wang, W. Q. Cao, H. L. Shi, M. M. Lu, G. Wang, H. B. Jin, W. Z. Wang, J. Yuan and M. S. Cao, Nanoscale, 2014, 6, 5754–5761.
[72] X.L. Shi, M.S. Cao, J. Yuan, Q.L. Zhao, Y.Q. Kang, X.Y. Fang, Y.J. Chen, Applied Physics Letters., 93 (2008) 183118
[73] Y. Naito, K. Suetake, IEEE Trans. Microwave Theory Tech., 19 (1971) 65.
[74] Y. Zhang, Z. Huang, F. Tang, and J. Ren, Thin Solid Films., 515 (4) (2006) 2555
[75] A. R. Bueno, M. L. Gregori, and M. C. S. Nobrega, Journal of Magnetism and Magnetic Materials., 320 (6) (2008) 864
[76] X. H. Li, H. B. Yi, J. W. Zhang, J. Feng, F. S. Li, D. S. Xue, H. L. Zhang, Y. Peng and N. J. Mellors, J. Nanopart. Res., 15 (2013) 1472
[77] T. H. Ting, R. P. Yu, and Y. N. Jau. Mater. Chem. Phys., 126 (2011) 364.
[78] S. H. Hosseini, S. H. Mohseni, A.Asadniac and H. Kerdari, J. Alloy. Compd., 509 (2011) 4682.
[79] K. Y. Chen, C. Xiang, L. C. Li, H. S. Qian, Q. S. Xiao and F. Xu. J. Mater. Chem., 22 (2012) 6449.
[80] Z. F. He, Y. Fang, X. J. Wang and H. Pang, Synth. Met., 161 (2011) 420.
[81] C. M. Yang, H. Y. Li, D. B. Xiong, and Z. Y. Cao, React. Funct. Polym., 69 (2009) 137.
[82] Seyed Hossein Hosseini and Ahmad Asadnia. Volume 2012, Article ID 198973, 6 pages
[83] Na Chen, Mingyuan Gu. Open Journal of Metal, 2 (2012)37
[84] Juhua Luo, Yang Xu, Duoduo Gao., Solid State Sciences 37 (2014) 40
[85] X. Tang and Y. G. Yang, Appl. Surf. Sci., 255 (2009) 9381.
[86] C. K. Cui, Y. C. Du, T. H. Li, X. Y. Zheng, X. H. Wang, X. J. Han and P. Xu, J. Phys. Chem. B., 116 (2012) 9523.

